Sliding Mode Controller for a Quadrotor

by

Robin Thomas
B.Eng., Anna University, India, 2010

A Report Submitted in Partial Fulfillment
of the Requirements for the Degree of

MASTER OF ENGINEERING

in the Department of Mechanical Engineering

Sliding Mode Controller for Quadrotor

by

Robin Thomas
B.Eng., Anna University, India, 2010

Supervisory Committee

Dr. Yang Shi (Supervisor)
Department of Mechanical Engineering

Dr. Ben Nadler (Committee Member)
Department of Mechanical Engineering

Supervisory Committee

Dr. Yang Shi (Supervisor)
Department of Mechanical Engineering

Dr. Ben Nadler (Committee Member)
Department of Mechanical Engineering

Abstract

Quadrotor is one type of Unmanned Aerial Vehicle (UAV) capable of vertical take-off and landing (VTOL). In this project, the well-established Sliding Mode Control (SMC) approach is studied and applied to a quadrotor to control the horizontal movement along the x-axis. The SMC design starts with appropriately defining a desired sliding surface containing the desired system dynamics on which the system states are expected to slide. System states will converge and reach the sliding surface by following the sliding mode control law thereby stabilizing the quadrotor position. Further, in order to suppress the severe chattering, a positive constant is introduced to the denominator term in the control law. A set of simulation studies are run to obtain relatively better values for this positive constant and the gain. Comprehensive simulation and comparison studies are then illustrated to show the improved performance over LQR control.

Contents

List of Tables

List of Figures

Acknowledgement

First of all, I would like to express my sincere gratitude to my supervisor Dr. Yang Shi. He is the reason that I was able to acquire some knowledge in control systems which was my goal when I decided to do masters. From the point of admission to completion of my program, Dr. Shi was patient enough and let me gradually learn the concepts. He gave me the opportunity to work on this exciting project in which I have always fascinated about and where I could learn a lot. I am also grateful to him that he provided me the opportunity to work with an aerospace company as a co-op student. I personally believe that the amount of respect and support from my lab mates shows more of Dr. Shi's supervision and support. It has been a privilege to complete my master's degree under his supervision.

Secondly, I am very thankful to BingXian Mu and Kunwu Zhang for their complete support even in between their busy schedule. They helped me to accelerate my project towards completion and they have always been good friends and advisors to me. I also acknowledge the support of other lab mates who always provided me with a friendly atmosphere during my time at the university. I would also like to thank Mehran Farhan Manesh for his suggestions and informative discussions which helped me to understand certain concepts of control system.

I am indebted to the professors and Instructors at University of Victoria from whom I have obtained knowledge through learning and doing projects. I have gained skills from projects done with Dr. Zuomin Dong, Dr. Nikolai Dechev, Dr. Stephanie Willerth, Dr. Armando Tura, Patrick Chang and Bill Bird.

Finally, I would like to thank my parents and brother who believed in my ideas, respected my desires in life and supported me mentally and financially.

Above all, I am always thankful to god who is works through me.

Dedication

I would like to dedicate my work to my parents and my brother who supported and believed in me.

Abbreviation

UAV	Unmanned Ariel Vehicle
VTOL	Vertical Takeoff and Landing
SMC	Sliding Mode Controller
ISMC	Integral Sliding Mode Controller
LQR	Linear Quadratic Regulator
PD	Proportional Derivative
PID	Proportional Integral Derivative
DAQ	Data Acquisition
HiQ	Quarc Aerial Vehicle data Acquisition Card (DAQ)
PWM	Pulse Width Modulation
TTL	Transistor-Transistor Logic
GPS	Global Positioning System
LiPo	Lithium Polymer
TCP/IP	Transmission Control Protocol / Internet Protocol
VGA	Video Graphics Array
USB	Universal Serial Bus
RPM	Rotation Per Minute
LTI	Linear Time-Invariant
DOF	Degree of Freedom
MSE	Mean Square Error

Nomenclature

E- Frame	Earth Fixed Frame
B- Frame	Body Fixed Frame
$O_B, \mathrm{x}, \mathrm{y}, \mathrm{z}$	Origin on body frame
$O_E, \mathrm{X}, \mathrm{Y}, \mathrm{Z}$	Origin non earth fixed frame
CoG	Center of Gravity
Ω_H	Motor speed (RPM)
a_1, a_2, a_3	Linear independent vectors on E-Frame to show transformation
b_1, b_2, b_3	Linear independent vectors on B-Frame to show transformation
R	Rotational Matrix
θ	Pitch Angle
φ	Roll Angle
Ψ	Yaw Angle
Γ	Transformation
ω	Angular Velocity of E-frame
v	Linear Velocity
p,q,r	Angular velocity of B-Frame
m	mass
F	Force
ξ(t,x)	Disturbance
G	Switching Matrix
$f_u(t,x)$	Unmatched Uncertainty
$\sigma(t)$	Sliding surface
$u_0(t)$	Linear Control input
$u_n(t)$	Non-Linear Control Input
ρ	Modulation Gain
x	Position in x- axis
$\dot{x}$	Velocity in x- axis

θ	Angular Position of pitch angle
$\dot{\theta}$	Angular Velocity of pitch angle
v_θ	Actuator Dynamics
δ	Positive Constant

Chapter 1

Unmanned Aerial Vehicle (UAV)

1.1 Introduction

This chapter provides information about the origin and description of Unmanned Ariel Vehicles (UAV), specifically Quadrotors. It also contains information on categorization of UAV's into fixed wing and Rotary wings along with its sub classification. UAV's are aircrafts without a human pilot aboard. Operation UAV's consists of UAV, a ground-based controller and a system of communication as part of Unmanned Aircraft System (UAS). UAV's can be of different types which can be categorized as fixed wing, rotary wing and flapping wing. General Atomics MQ-9 Reaper [1] shown in figure 1 is a UAV capable of remotely controlled or autonomous flight operations. It is powered by 950-shaft-horsepower (712 KW) Turboprop engine. In fixed winged UAV structures, a lift is produced under the wings on the runway allowing it to takeoff. Therefore fixed wing UAV's requires a runway for takeoff and landing. The mechanics of rotary-wing UAV's are complex than a fixed wing as it is capable of Vertical Takeoff and Landing (VTOL).

Figure 1: General Atomics MQ-9 Reaper [1]

Rotary wing UAV's varies based on the number of propellers. It ranges from a 2-rotor helicopter to multi-rotor UAV's. Most common ones under rotary winged ones are Quadrotor, Hexacopter and Octocopter [2]. Quadrotor was first constructed by two brothers Louis Breguet and Jacques Breguet under the guidance of Professor Charles Richet which was named as Breguet Richet Gyroplane No.1 in 1907. Quadrotor is a Vertical Takeoff or Landing vehicle (VTOL) which makes it exceptional when it comes to Unmanned Ariel Vehicle (UAV) applications in dangerous and unsafe environment by virtue of its supermaneuvrability. [3] Quadrotors are used in areas such as

search and rescue and emergency response, homeland security, military surveillance and earth sciences. Moreover, they can also be used to study climate change, glacier dynamics, volcanic activities and for atmospheric sampling. The limitations and delay of ground robots has been compensated by the use of Ariel robots like Quadrotors. Therefore, large scale research and funding started going into civilian and military markets. Parrot AR Drone 2.0 [4] shown in figure 2 is a quadrotor which provides piloting functions and ability to capture photos and videos. It provides piloting capabilities via IOS and android devices. It is propelled by four in runner type brush-free motors of 14.5 watts and 25,500 rev/min and stabilized using 3-axis gyroscope, accelerometer and magnetometer. Based on widespread application of Quadrotors, the chapter discusses the significance of research on control system on Quadrotors as well.

Figure 2: Parrot AR Drone 2.0 [4]

1.2 Motivation

Quad-rotors are very useful tool for university researchers to test new control systems on flight control theory, navigation, real-time systems and robotics. Flying robots or vehicles has always been exciting and a great fascination for people. For many years, Control system on Unmanned Ariel Vehicle (UAV) has become a challenging area of research and an area which demands continuous improvements. Quadrotors offer a challenging problem due to highly unstable nature. The system requires fast control response and large operation range. Some of the challenges in Quadrotor control are: they demands strong coupling between its dynamic states for positioning and calculation. Some parameters associated with Quad-rotor dynamic model such as inertial moments and aerodynamic coefficients cannot be obtained precisely. Besides, they are very

sensitive to external disturbances from the flying environment due to small size and weight of the Quad-rotor. An effective control system is required to control such a unique system.

1.3 Review of Control System

Several linear control approaches such as PD controller and Proportional Integral Derivative (PID) been applied to attitude stabilization and attitude tracking of quadrotors and Linear Quadratic Regulators (LQR) for the linearization of dynamics. [5] But these control strategies might impose limitations during extended flight and aggressive maneuvers where the system dynamics can be non-linear and moreover the stability of the quadrotor can only be guaranteed around the equilibrium point. However in this project, LQR is used to obtain the control gain for linear input to assist sliding mode controller during simulation PD and PID controllers will assist Sliding mode control system by controlling the altitude and yaw angle during the experiments.

1.3.1 Existing Control System on Qball X4 quadrotor

As the scope of this project, a sliding mode control is implemented to the quadrotor dynamics to analyze the system state response to the control system. The project is based on published work by BingXian and Dr. Yang Shi [6]. They implemented Integral Sliding Model Control (ISMC) to Qball X4 quadrotor and experimented it to analyze rejection of matched and unmatched uncertainties. [6] Their experiments were conducted on a control platform split into two control systems, the attitude and the position control. Based on the linearized equations, the motion of the quadrotor in the x and y plane depends on the roll and pitch movement. A PID and PD controller is used to regulate the altitude and the Yaw angle. A standard Linear Quadratic Regulator (LQR) is used to obtain the gain value to linearize quadrotor dynamics. LQR Control is designed by operating a dynamics system by minimizing a suitable cost function. It is used to minimize small errors. Q is a positive definite matrix weighting the size of the state responses. [5]

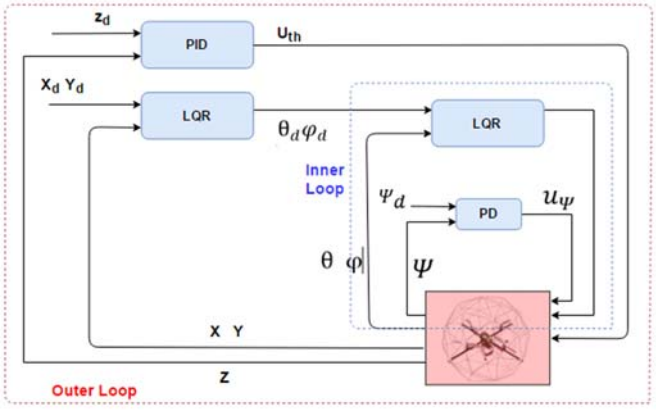

Figure 3: Existing Feedback control loop for Qball [5]

$x, y, z, \theta, \varphi, \Psi$ are the measured states and $x_d, y_d, z_d, \theta_d, \varphi_d, \Psi_d$ are the desired states. An optimum gain can be obtained as shown in the following derivation. Consider the following continuous-time Linear Time Invariant (LTI) system defined on $\mathrm{t} \in [0, t]$

$$\dot{x} = \mathrm{Ax} + \mathrm{Bu} \tag{1.1}$$

with a quadratic cost function defined as follows:

$$J = \int_0^t (x(\tau)^T Qx(\tau) + u^T(\tau)Ru(\tau))d\tau \tag{1.2}$$

where $x \in \mathbb{R}^n and\ u = \mathbb{R}^m$ the system state input. $A \in \mathbb{R}^{n\times n}, B \in \mathbb{R}^{n\times m} and\ C \in \mathbb{R}^{p\times m}$ are the state matrix, input matrix and the output matrix, $Q \in \mathbb{R}^{n\times n}\ and\ R \in \mathbb{R}^{m\times m}$ are positive definite weighting matrices for the states and the inputs. If matrices A and B are controllable, the states are available, the feedback control that minimizes the value of the cost is

$$u = -kx \tag{1.3}$$

where $K = R^{-1}B^T P$

P , a positive-definite symmetric matrix, can be obtained as a unique solution of continuous time Riccati differential equation

$$A^T P + PA - PBR^{-1}B^T P + Q = 0 \tag{1.4}$$

1.4 Outline

The report is organized as follows:

- Chapter 1 introduces the types of Unmanned Ariel Vehicles and the control system approaches on Quadrotors. The significance of Unmanned vehicles and the challenging applications of vertical takeoff and landing are also mentioned in chapter 1. In Section 1.3, a review of existing control system on Qball X4 quadrotor is also discussed.
- Chapter 2 introduces Quarc Qball Quadrotor system, its components and communication with target vehicle. In the following sections, System modelling, Kinematics of Quad-rotor, Dynamics of Quadrotor and the simplified quadrotor dynamics equations are also formulated is explained.
- Chapter 3 provides the derivation of mathematical model of Sliding mode controller for quadrotor dynamics in section 3.1, 3.2 and 3.3 followed by modelling of a Simulink model of SMC in section 3.5 and simulations in section 3.6.
- Chapter 4 reviews the existing ISMC system on Qball X4. The control system equations are derived and ISMC model is simulated for ideal results which is displayed in 4.8.
- Chapter 5 concludes with a brief summary of the project, advantages and disadvantages of Sliding Mode Control System in section 5.1 and Future Works in section 5.2.

Chapter 2

Quanser Qball-X4

2.1 Introduction

The Quanser Qball is a rotary wing vehicle platform suitable for UAV research applications propelled by four 10-inch propellers. It is covered by a protective carbon fibre cage to prevent damage to the on board hardware from potential close range hazards since it is used in an indoor lab setup. It uses Quanser on-board avionics data acquisition card (DAQ), HiQ and the embedded Gumstix computer to measure the sensors and data to drive the motors. HiQ DAC is a high resolution inertial measurement unit. Quarc is a real-time control software from Quanser to test control systems on hardware through MATLAB Simulink interface. [7] [8]

Figure 4: Qball X4 Quadrotor [7]

The frame of the Quadrotor is a cross-beam structure on which the components are mounted. The components include HiQ DAQ, motors and speed controllers.

2.2 Components of Qball Quadrotor

2.2.1 HiQ DAQ

HiQ DAQ is the Quad-rotors data acquisition board with the Gumstix embedded computer. Using the data it can control the vehicle by reading the onboard sensors and output motor commands. HiQ includes 10 PWM servo output channels, 3-axis accelerometer, 6-analog inputs, 3-axis

magnetometer, 8-channel RF receiver inputs. It has another daughter board attached to it that can provide provision to sonar input-output features, TTL serial inputs, GPS receiver etc.

2.2.2 Power Supply

The Q-ball X-4 makes used of 3-cell 2500mAh LiPo batteries to power HiQ and the motors attached in a battery compartment beneath the cross frame by using Velcro straps. Each pair of motors are powered with one battery

2.2.3 Motors and Propellers

The Quad-rotor uses four E-Flight park 480 (1020 Kv) motors with paired counter rotating APC 10x4.7 propellers. The propellers are fixed on the four motors and the motors are fixed on the frame in X and Y axis. Motors are connected to four speed controllers fixed on to the frame. Electronic Speed Controllers are fed with PWM signals from HiQ.

2.2.4 Qball joystick

The joy stick is used to fly the Quadrotor using two controller sticks of actuation. It is used to actuate the throttle for roll, pitch, yaw and hovering conditions. In autonomous mode, joystick has to be used to initialize and kill the control in case it goes unstable and the Quad-rotor has to be stopped.

2.2.5 Wireless communication

Q-Ball uses as-hoc peer-to-peer wireless TCP/IP to connect to host computer or Quanser unmanned vehicles. The host PC and the vehicle must have the same IP addressees. The hardware kit comes with a USB wireless adapter to setup the host computer with wireless connection. In Quarc software, IP address of the target vehicle should be specified. When Simulink is set to working in the external mode, the model will run on the Quarc target.

2.2.6 Localization System

Experiments are conducted in indoor facility. Therefore using Global Positioning System will not be effective. OptiTrack system from Natural Point Inc. is used to capture the motion of the QBall Quadrotor. The system is a vision based localization system including several OptiTrack cameras. There are reflective markers on the system with a specific configuration in which the cameras can detect. For the system to track six degree of freedom, the quadrotor needs four reflective markers. The manufacturer has provided a software called Motive for calibration procedure.

The cameras used in the Optitrack vision system is OptiTrack Flec 3 cameras. These are cameras capable of capturing and processing integrated images with 100 frames per capture speed

and 640x480 VGA solution. The tracking data will be recorded in the QUARC OptiTrack block in Simulink to provide position information. The lab of volume 4.21m x 4.06m x 2.74m is equipped with 10 cameras mounted on the wall connected to two Optihubs to facilitate a workspace volume of 1.5m x 1.5m x1.5m.

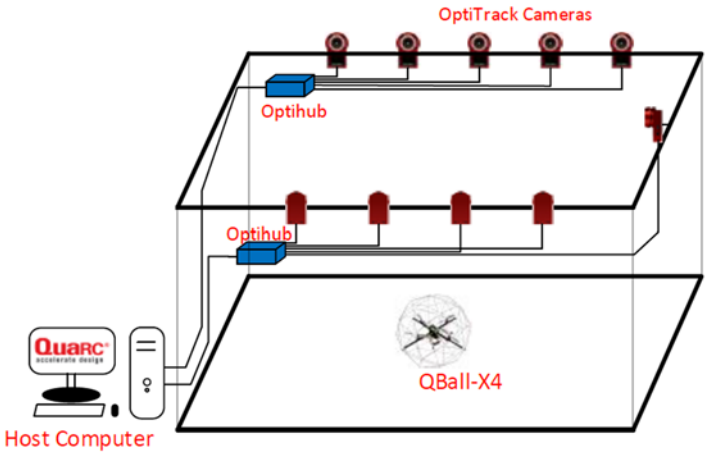

Figure 5: Lab Setup [5]

2.3 System Modelling

Quadrotor is a type of multirotor with four motors used as propellers. They are mounted on a crossbeam by maintaining equal distance between each other. The rotors work in pairs such as two of the motors work in the opposite direction to the other two to stabilize the rotary torque induced by all the motors. The two pairs of propellers has opposite blade pitch angles so that thrust generated by each propeller is applied towards the same direction.

2.3.1 Kinematics of Quad-rotor

The movement of Quad-rotor will be based two frames of which, one will be fixed on the earth called the E-frame and the other fixed on the body frame called as B-frame. This is setup to realize the transition of Quadrotor movement based on a fixed reference frame (x,y,z) to the origin of the body fixed frame O_B as shown in *Figure 1*.

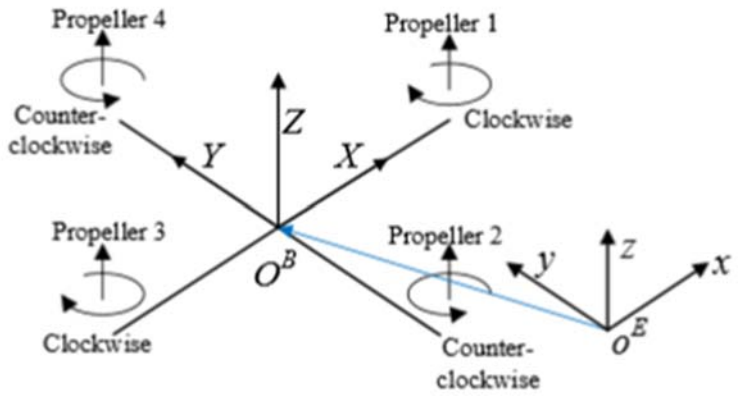

Figure 6: The body frame and the inertial frame [9]

During hovering condition all the four propellers will be driven in the same speed Ω_H and the total thrust produced will be equal to cancel out the gravitational force by accelerating in z-axis. From the thrust vs RPM curve you can calculate the operating speed of the motor. The motors are selected in such a way the torque produced will be able to overcome the drag moment.

To describe 3-D displacements of motion of rigid bodies through space, both position and orientation has to be described. The position of the Quadrotor which is moving from one point to the other in space, can be defined based on an E-frame, also known as inertial frame. Linear independent vectors on E-frame and B-frame are a_1, a_2 and a_3 and b_1, b_2 and b_3. The transformation of vectors from one frame to the other can be obtained using a rotational matrix.

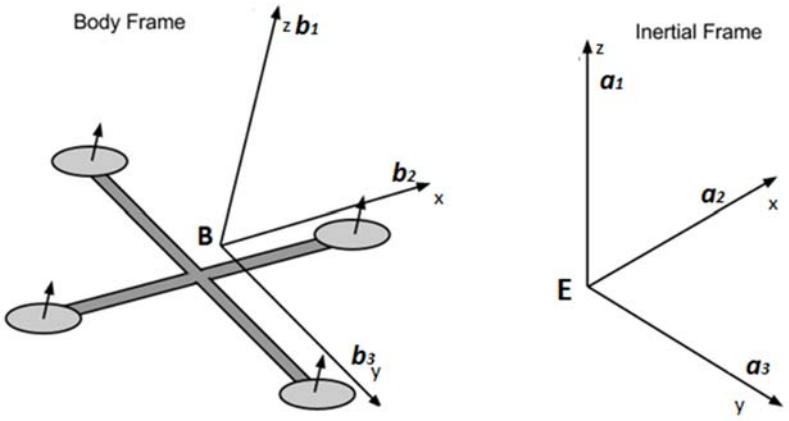

Figure 7: Linear independent vectors [9]

Rotational matrix of Quad-rotor can be written by writing mutually orthogonal unit vectors in one frame as linear combinations of mutually orthogonal vectors of the other frame.

Properties of rotational matrix are as follows:

- Rotational matrices are orthogonal
- Determinant will be one
- Product of two matrices will be a rotational matrix
- The inverse of a rotational matrix will be a rotational matrix

The transformation from E-frame to B-frame can be defined as follows:

$$b_1 = R_{11}a_1 + R_{12}a_2 + R_{13}a_3 \tag{2.1}$$

$$b_2 = R_{21}a_1 + R_{22}a_2 + R_{23}a_3 \tag{2.2}$$

$$b_3 = R_{31}a_1 + R_{32}a_2 + R_{33}a_3 \tag{2.3}$$

Rotational Matrix,

$$R = \begin{bmatrix} R_{11} & R_{12} & R_{13} \\ R_{21} & R_{22} & R_{23} \\ R_{31} & R_{32} & R_{33} \end{bmatrix} \tag{2.4}$$

Therefore, rotation of Quad-rotor on (xyz) axis through angles θ, φ and Φ can be defined as the following rotational matrices corresponding to rotational movements.

Total thrust vector can be considered as input U_1 to the control system and the net moment as U_2

The control system includes three components of position, velocity and acceleration and three components of rotations, angular velocities and angular accelerations.

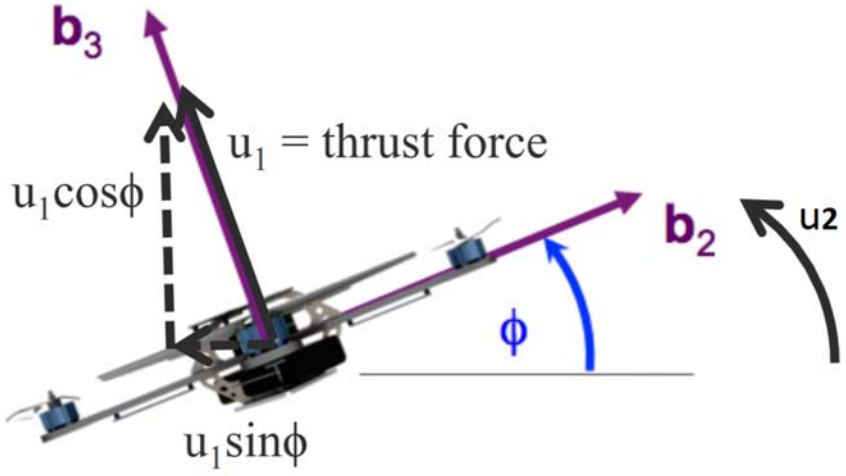

Figure 8: Angular Motion

- Roll angle, φ

Roll movement is generated when the Quad-rotor rotates on x-axis with an angle, φ. When the speed of the rotors 2 and 4 decreases or increases generating corresponding thrust, the Quad-rotor

will roll on x-axis. Same as the pitch movement the hovering condition will be maintained when the vertical component along x-axis is maintained. The rotation of the Quad-rotor on x-axis with respect to E-frame can be defined by the following rotational matrix.

$$\Gamma^E = R(x, \varphi)\Gamma^B \tag{2.5}$$

$$R(x, \varphi) = \begin{bmatrix} 1 & 0 & 0 \\ 0 & cos\varphi & -sin\varphi \\ 0 & sin\varphi & cos\varphi \end{bmatrix} \tag{2.6}$$

- Yaw angle, Ψ

The rotation of the Quad-rotor on z-axis with an angle, Ψ induces a Yaw movement on the Quad-rotor. Rotation around z-axis can be obtained by increasing or decreasing the thrusts of rotors 1 and 3 and by increasing or decreasing the speed of rotors 2 and 4 with respect to the speed of rotors 1 and 3. The torque produced will favour the Quad-rotor to rotate on z-axis. To maintain hovering state, the thrusts of the Quad-rotor will have the same magnitude in the opposite direction of the gravitational force. The rotation of the Quad-rotor on z-axis with respect to E-frame can be defined by the following rotational matrix.

$$\Gamma^E = R(z, \psi)\Gamma^B \tag{2.7}$$

$$R(z, \psi) = \begin{bmatrix} cos\psi & -sin\psi & 0 \\ sin\psi & cos\psi & 0 \\ 0 & 0 & 1 \end{bmatrix} \tag{2.8}$$

- Pitch angle, θ

The rotation of the Quad-rotor on y-axis will be with an angle, θ which will induce a Pitch movement. Pitch can be obtained by increasing or decreasing the thrusts of rotors 1 and 3, by controlling its speed. In this case, a torque around y-axis is induced, allowing the Quad-rotor to pitch on either sides on Y-axis with respect to the input. Hovering condition is maintained in line with the pitch movement when the vertical component of the thrust along the y-axis is generated. The rotation of the Quad-rotor on y-axis with respect to E-frame can be defined by the following rotational matrix.

$$\Gamma^E = R(y, \theta)\Gamma^B \tag{2.9}$$

$$R(y, \theta) = \begin{bmatrix} cos\theta & 0 & sin\theta \\ 0 & 1 & 0 \\ -sin\theta & 0 & cos\theta \end{bmatrix} \tag{2.10}$$

Based on Euler angle convention, the position of quad-rotor can be transformed into E-frame by

$$\Gamma^E = R_{B,E}\Gamma^B \tag{2.11}$$

Rotation matrix from B frame to E frame,

$$R_{BE} = R(z\,\psi).R(y\,\theta).R(x\,\varphi) \tag{2.12}$$

$$R_{B,E} = \begin{bmatrix} c\theta c\psi & s\varphi c\theta c\psi - c\varphi s\psi & c\varphi c\psi s\theta + s\varphi s\varphi \\ s\psi c\theta & s\varphi s\theta s\psi + c\varphi c\psi & c\varphi s\varphi s\theta - s\varphi c\psi \\ -s\theta & s\varphi c\theta & c\varphi c\theta \end{bmatrix} \tag{2.13}$$

Relation of rotational matrices between E frame and B frame can be given as $R_{EB} = R_{BE}^{-1} = R_{BE}^{T}$. Linear velocities in E frame and B frame are $V^E = R_{BE}V^B$. Angular velocities of E frame to B frame $\omega^E = T_{BE}\omega^B$

Transformational matrix T_{BE} can be derived from the following equation

$$\begin{bmatrix} p \\ q \\ r \end{bmatrix} = \begin{bmatrix} \dot{\varphi} \\ 0 \\ 0 \end{bmatrix} + R(x,\varphi)^{-1} \begin{bmatrix} 0 \\ \dot{\theta} \\ 0 \end{bmatrix} R(x,\varphi)^{-1}R(y,\theta)^{-1} \begin{bmatrix} 0 \\ 0 \\ \dot{\psi} \end{bmatrix} \tag{2.14}$$

By solving the above equation (2.14)

$$T_{BE}^{-1} = \begin{bmatrix} 1 & 0 & -sin\theta \\ 0 & cos\varphi & cos\theta sin\varphi \\ 0 & -sin\varphi & cos\theta cos\varphi \end{bmatrix}, \tag{2.15}$$

$$T_{BE} = \begin{bmatrix} 1 & sin\varphi tan\theta & cos\varphi tan\theta \\ 0 & cos\varphi & -sin\varphi \\ 0 & \dfrac{sin\varphi}{cos\theta} & \dfrac{cos\varphi}{cos\theta} \end{bmatrix} \tag{2.16}$$

From equations of linear Velocity V^E and Angular Velocity ω^E Kinematic equation of quadrotor can be written as

$$\begin{bmatrix} \mathrm{V^E} \\ \omega^{\mathrm{E}} \end{bmatrix} = \begin{bmatrix} R_{BE} & O_{3\times3} \\ O_{3\times3} & T_{BE} \end{bmatrix} \begin{bmatrix} \mathrm{V^B} \\ \omega^{\mathrm{B}} \end{bmatrix} \tag{2.17}$$

2.3.2 Dynamics of Quadrotor [5]

Thera are four rotors that are independently actuated. Reaction moments are proportional to the angular speeds of the rotor. Every rotor handles approximately $\frac{1}{4}$ of the total weight of the Quad-rotor. There is a quadratic relation between the speed of the rotor and the thrust which is $F = K_F\omega^2$ where K_F is the proportionality constant, $\mathrm{F_i} = \mathrm{k_F}\omega_{\mathrm{i}}^2$ *and the reaction moment* $\mathrm{M_i} = \mathrm{k_M}\omega_{\mathrm{i}}^2$

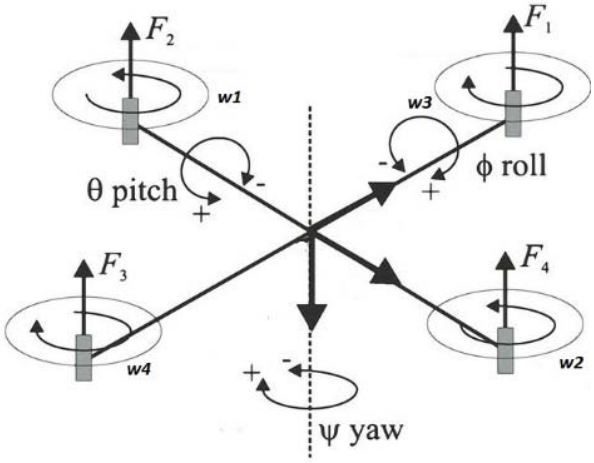

Figure 9: Forces acting on a Quadrotor [10]

The total force acting on the Quad-rotor is sum of the four thrust = vectors and the gravity vector $F = F_1 + F_2 + F_3 + F_4 - mga_3$. The sum of moments are obtained by adding the reaction forces and the moments of the truss forces, $M = r_1 \times F_1 + r_2 \times F_2 + r_3 \times F_3 + r_4 \times F_4 + M_1 + M_2 + M_3 + M_4$. The movement of the Quad-rotor is based on the center of mass. Center of mass can be obtained by dividing the weighted sum of all position vectors $\mathrm{r_c} = \frac{1}{\mathrm{m}} \sum_{\mathrm{i=1,N}} \mathrm{m_i}\, \mathrm{P}$, where P is Position vectors.

The rate of change of angular moment of a rigid body is equal to the resultant moment of all external forces acting on the body, $\frac{\mathrm{d}}{\mathrm{dt}} \mathrm{H} = \mathrm{M}$, where H-Angular Momentum and M is the Net moment. Angular Momentum is the product of Inertia and angular velocity, $\mathrm{H} = \mathrm{I} \times \omega$. Quadrotor equations of motion can be formulated using Newton-Euler equations by combining the net forces and the net moments. Acceleration is obtained by Newton's second law, the total force equals mass times acceleration a. The rotational matrix R rotates the thrust vector to the inertial frame.

Motion of a quadrotor with respect to the B frame can be explained based on Newton-Euler equations. Dynamics of the linear motion of quadrotors are as follows:

From [5] Based on newton 2nd law of motion, Force on the earth fixed frame and force on the body fixed frame can be explained as follows:

$$F_E = m \frac{d}{dt}(V_E), \tag{2.18}$$

$$F_B = m(\dot{V}_B + \omega_B \times V_B) \tag{2.19}$$

where m is mass of the Quadrotor, F_E and F_B are the forces acting on the quadrotor expressed in E-Frame and B-Frame respectively.

From the Euler equations, quadrotor dynamics of the angular rotation can be derived as

$$\tau_E = J\frac{d}{dt}\omega_E \tag{2.20}$$

$$\tau_B = J(\dot{\omega}_B + \omega_B \times \omega_B) \tag{2.21}$$

2.3.3 Force Calculation [5]

Main forces acting on the Quadrotor are the thrust force generated by the motors, F_T, the drag force F_D, gravity F_G and the hub force acting on the blades due to the horizontal forces acting on the blades of the rotor. Hub force is neglected due to negligible force of air as the quadrotors are operated in closed facility in the lab.

- Gravitational force F_G

Gravity force $F_G = [0 \quad 0 \quad mg]^T$ acts along the negative z-axis on the E-frame. Gravitational force can be expressed in B-frame as follows:

$$F_G = R_{EB}\begin{bmatrix} 0 \\ 0 \\ mg \end{bmatrix} = \begin{bmatrix} -mgsin\theta \\ mgsin\varphi cos\theta \\ mgcos\varphi cos\theta \end{bmatrix} \tag{2.22}$$

- Drag force

Drag force can be written as follows:

$$F_D = \frac{1}{2}C_D S_\rho R_{EB} V^B = \begin{bmatrix} \frac{1}{2}C_{Dx}S_{\rho u} \\ \frac{1}{2}C_{Dx}S_{\rho v} \\ \frac{1}{2}C_{Dx}S_{\rho w} \end{bmatrix} \tag{2.23}$$

where $C_{Dx}, C_{Dy}\ and\ C_{Dz}$are the drag coefficients along x, y and z axis in the E-frame, S is the cross-section and ρ is the air density

- Thrust force

Thrust force is generated by each propeller independently parallel to the z-axis. Total thrust generated by all the motors can be written as follows:

$$F_D = \begin{bmatrix} 0 \\ 0 \\ \tau^B \end{bmatrix}, \tag{2.24}$$

where $T^B = F_{T1} + F_{T2} + F_{T3} + F_{T4}$

The drag force is neglected in the dynamics equation formulation as relatively very less than the thrust force and the gravitational force.

Therefore from Eq. 2.19 Dynamic equations can be written as follows:

$$m\dot{u} + m(qw - rv) = -mgsin\theta, \tag{2.25}$$

$$m\dot{v} + m(ru - pw) = mgsin\psi cos\theta, \tag{2.26}$$

$$m\dot{w} + m(pv - qu) = mgcos\psi cos\theta + \tau^B \tag{2.27}$$

where u, v and w are linear velocities and p,q and r are angular velocities

2.3.4 Torque Calculation [5]

Torque is generated by the four propellers attached to the motors. Desired input can be given to the Quadrotor for pitch, roll and yaw movements. The pitch and roll can be calculated by using the following equations:

$$T_\theta = l(F_{T1} - F_{T3})$$

$$T_\varphi = l(F_{T2} - F_{T4})$$

where l is the distance between propeller and CoG

The torque generated to maintain Yaw can be written as follows:

$$\tau_\psi = \tau_1 + \tau_2 + \tau_3 + \tau_4 \tag{2.28}$$

The inertia tensor j can be expressed as

$$J = \begin{bmatrix} J_{xx} & J_{xy} & J_{xz} \\ J_{yz} & J_{yy} & J_{yz} \\ J_{zx} & J_{zy} & J_{zz} \end{bmatrix}, \tag{2.29}$$

since quadrotor geometry is symmetric, $J_{xy} = J_{xz} = J_{yx} = J_{yz} = J_{zx} = J_{zy} = 0$ and therefore inertia tensor can be re-written as

$$J = \begin{bmatrix} J_{xx} & 0 & 0 \\ 0 & J_{yy} & 0 \\ 0 & 0 & J_{zz} \end{bmatrix} \tag{2.30}$$

From Eq. 2.21, Dynamics equations can be formulated as follows:

$$J_{xx}\dot{P} + qr(J_{zz} - J_{yy}) = l(F_{T1} - F_{T3}), \tag{2.31}$$

$$J_{yy}\dot{q} + pr(J_{xx} - J_{zz}) = l(F_{T2} - F_{T4}), \tag{2.32}$$

$$J_{xx}\dot{r} + pq\left(J_{yy} - J_{xx}\right) = \tau_1 + \tau_2 + \tau_3 + \tau_4 \tag{2.33}$$

where u, v and w are linear velocities and p, q and r are angular velocities.

To explain the angular movement of the Quad-rotor, the planar movement on Y-Z plane can be analyzed and explained. It is assumed there is no movement in the x- direction and no yaw or pitch motions. From Eq. 2.33, 2.34, 2.35, 2.42, 2.43, 2.44. Therefore quadrotor dynamics of B-frame can be written as:

$$\dot{u} - gsin\theta - (q\omega - rv), \tag{2.34}$$

$$\dot{v} = gsin\psi cos\theta - (ru - p\omega), \tag{2.35}$$

$$\dot{w} = gcos\psi cos\theta + \frac{T_B}{m} - (pv - qu), \tag{2.36}$$

$$\dot{p} = \frac{l(F_{T1} - F_{T3})}{J_{xx}} - \frac{qr(J_{zz} - J_{yy})}{J_{xx}}, \tag{2.37}$$

$$\dot{q} = \frac{l(F_{T2} - F_{T4})}{J_{yy}} - \frac{pr(J_{xx} - zz)}{J_{yy}}, \tag{2.38}$$

$$\dot{r} = \frac{\tau_1 - \tau_3 - \tau_2 - \tau_4)}{J_{zz}} - \frac{pq(J_{yy} - J_{xx})}{J_{zz}} \tag{2.39}$$

Angular velocities in the B-frame and E-frame of the Quadrotor while hovering at a lower altitude is considered approximately equal.

$$(\dot{\varphi}, \dot{\theta}, \dot{\psi}) \approx (p, q, r) \tag{2.40}$$

Quadrotor dynamics in the E-frame can also be obtained from $R_{BE}F_B = m\frac{d}{dt}(V_E)$ and written as follows:

$$\ddot{x} = \frac{T^B}{m}(cos\varphi sin\psi + cos\varphi sin\theta cos\psi), \tag{2.41}$$

$$\ddot{y} = \frac{T^B}{m}(-sin\varphi cos\psi + cos\varphi sin\theta cos\psi), \tag{2.42}$$

$$\ddot{z} = \frac{T^B}{m}cos\varphi cos\theta - g, \tag{2.43}$$

$$\ddot{\varphi} = \frac{l(F_{T1} - F_{T3})}{J_{xx}} - \frac{\dot{\theta}\dot{\psi}(J_{zz} - J_{yy})}{J_{xx}}, \tag{2.44}$$

$$\ddot{\theta} = \frac{l(F_{T2} - F_{T4})}{J_{yy}} - \frac{\dot{\varphi}\dot{\psi}(J_{xx} - J_{zz})}{J_{yy}}, \tag{2.45}$$

$$\ddot{\psi} = \frac{T_1 + T_3 - T_2 - T_4)}{J_{zz}} - \frac{\dot{\varphi}\dot{\theta}(J_{yy} - J_{xx})}{J_{zz}} \tag{2.46}$$

2.4 Simplified Quadrotor Dynamics [5]

As shown in the above equations, there are non-linearities in in the equations. Due to the non-linearities, the control system would be complex and difficult to design a control algorithm. Therefore the systems is simplified using some assumptions as follows:

1. The Quadrotor operates at near hovering condition
2. The orientations of the Quadrotor (pitch, yaw and roll angles) are small
3. The cross-coupling terms in the system dynamics are ignored

Since it is assumed that the Quadrotor fly's in near hovering condition, total thrust produced will be approximately equal to the gravitational force, $T^B \approx mg$ and due to small orientations he angles are approximated as sinθ ≈ θ, sinφ ≈ φ, sinΨ = Ψ, cosθ ≈ 1, cosφ ≈ 1, cosΨ ≈ 1

$$\ddot{x} = g\theta \tag{2.47}$$

$$\ddot{y} = -g\varphi \tag{2.48}$$

$$\ddot{z} = \frac{F}{m} - g \tag{2.49}$$

$$\ddot{\varphi} = \frac{\tau_\varphi}{J_{xx}} \tag{2.50}$$

$$\ddot{\theta} = \frac{\tau_\theta}{J_{yy}} \tag{2.51}$$

$$\ddot{\psi} = \frac{\tau_\psi}{J_{zz}} \tag{2.52}$$

Quadrotor dynamics including the motor dynamics. Thrust generated by the Q-ball-X4 can be modelled as a first-order system

$$F_i = K_m\, v = K_m \frac{\omega}{s+\omega} u_i, \tag{2.53}$$

where $u_i$is the input PWM signal to the i^{th} motor; ω indicates the motor bandwidth; v is the state variable representing the motor dynamics and $K_m$is a positive gain. Four control inputs for the system is defined as $u_{th}, u_\theta, u_\varphi \; and \; u_\Psi$. The total force and torque are defined as follows:

$$F = 4K_m \frac{\omega}{s+\omega} u_{th}, \tag{2.54}$$

$$\tau_\theta = 2K_m l \frac{\omega}{s+\omega} u_\theta \tag{2.55}$$

$$\tau_\varphi = 2K_m l \frac{\omega}{s+\omega} u_\varphi \tag{2.56}$$

$$\tau_\psi = 4K_n u_\psi \tag{2.57}$$

From equations (2.49 – 2.54) and (2.56 – 2.59), state-space form of the decoupled equations along the x, y and z axis can be written as

$$\dot{X} = A_x X + B_x \theta, \tag{2.58}$$

$$\dot{X_\theta} = A_\theta X + B_\theta u_\theta, \tag{2.59}$$

$$\dot{Y} = A_y Y + B_y \varphi, \tag{2.60}$$

$$\dot{Y_\varphi} = A_\varphi Y_\varphi + B_\varphi u_\varphi, \tag{2.61}$$

$$\dot{Z} = A_z \mathrm{Z} + B_z u_{th} + \Omega, \tag{2.62}$$

$$\dot{\psi} = A_\psi \psi + B_\psi u_\psi \tag{2.63}$$

where $X = [x, \dot{x}]^T$, $Y = [y, \dot{y}]^T$, $Z = [z, \dot{z}, v_z]^T$, $X_\theta = [\theta, \dot{\theta}, v_\theta]^T$, $Y_\varphi = [\varphi, \dot{\varphi}, v_\varphi]^T$, $\Psi = [\psi, \dot{\psi}]$,

$$A_x = A_y = A_\psi = \begin{bmatrix} 0 & 1 \\ 0 & 0 \end{bmatrix}, A_\theta = \begin{bmatrix} 0 & 1 & 0 \\ 0 & 0 & \frac{2K_m l}{I_{yy}} \\ 0 & 0 & -\omega \end{bmatrix}, A_\varphi = \begin{bmatrix} 0 & 1 & 0 \\ 0 & 0 & \frac{2K_m l}{I_{xx}} \\ 0 & 0 & -\omega \end{bmatrix}, A_z = \begin{bmatrix} 0 & 1 & 0 \\ 0 & 0 & \frac{4K_m}{m} \\ 0 & 0 & -\omega \end{bmatrix}, B_\theta =$$

$$B_\varphi = B_z = [0 \quad 0 \quad w]^T, B_x = [0, g]^T, B_y = [0, -g]^T, B_\psi = [0, \tfrac{4K_n}{I_{zz}}]^T \; and \; \Omega = [0 \quad -g \quad 0]^T$$

Since this project is selecting only movement of Quadrotor in x-axis, dynamic equations in state space form can be formed as follows:

$$x(t) = [x, \dot{x}, \theta, \dot{\theta}, v_\theta], \qquad A_x = \begin{bmatrix} 0 & 1 & 0 & 0 & 0 \\ 0 & 0 & g & 0 & 0 \\ 0 & 0 & 0 & 1 & 0 \\ 0 & 0 & 0 & 0 & \frac{2k_m l}{I_{xx}} \\ 0 & 0 & 0 & 0 & -\omega \end{bmatrix}, \qquad B_x = [0 \quad 0 \quad 0 \quad 0 \quad w]$$

The state-`space equations and the Quad-rotor specifications mentioned above are used for designing the sliding mode control system which will be explained in the Chapter 3.

Q-Ball X4 specifications [7] are obtained from the manufacturer manual as follows:

Parameter	*Value*	*Description*
K	*120 N*	*Gain for motor*
ρ	*15 rad/s*	*Actuator bandwidth*
J_{xx}	*0.03 kg.m²*	*Inertia around x-axis*
J_{yy}	*0.03 kg.m²*	*Inertia around y-axis*
J_{zz}	*0.04 kg.m²*	*Inertia around z-axis*
M	*1.4 kg*	*Mass of Quad-rotor*
d	*4 N.m*	*Moment scaling factor*
l	*0.2 m*	*Distance between the motor shaft and CoG*

Table 1: Qball X4 Parameters [7]

2.5 Conclusion

In chapter 2, system dynamics are derived to demonstrate how 6-DOF is achieved by the quadrotor. Initially, the kinematics of a quadrotor is provided to explain the relation of orientation of body fixed frame to the inertial frame by forming a rotational matrix for yaw, pitch and roll movements. Following with the kinematics, dynamics are derived to obtain the forces and torques acting on the quadrotor to achieve movement in 3-translational and 3-rotational movements. A plannar demonstration is provided in section 2.3.2 to explain how the angular forces are calculated. Finally, a simplified set of quadrotor dynamics are formulated in section 2.4.

Chapter 3

Sliding Mode Controller

3.1 Introduction

Sliding mode control (SMC) is a robust technique to handle sudden and large changes to system dynamics. The control strategy has many applications in motor control, aircraft and spacecraft control, process control and power system. It has become one of the useful tools to design controllers for systems with uncertainties. Sliding mode utilizes discontinuous feedback control laws to force the system states to reach a predefined sliding surface called sliding or switching surface. To achieve a sliding mode control objective, the system must be designed in such a way that it overcomes the uncertainties involved. There are two main advantages of using this strategy which are: as soon as the system is sliding on the sliding manifold, it behaves as reduced order system and secondly the dynamics of the system will be completely independent of the uncertainties and disturbances. [12]

3.2 Problem Statement

The design procedure of a sliding mode controller can be explained by considering an uncertain linear time invariant (LTI) system of the following form.

$$\dot{x} = Ax(t) + B\dot{u}(t) + M\xi(t,x) \tag{4.1}$$

where $A \in \mathbb{R}^{n\times n}$ and $B \in \mathbb{R}^{n\times m}$

Assumption 1: (A,B) pair is controllable.

Assumption 2: $M \in \mathbb{R}^{n\times l}$ is known and lies in the range space of the input distribution matrix B. Therefore it is possible to write $M = BD$ for some $D \in \mathbb{R}^{m\times l}$. The function $\xi(t,x)$ is an external disturbance with an upper bound for all x and t. The uncertainty in the system can be considered as a matched uncertainty as it is acting the channel of the input distribution matrix. Therefore the uncertain system Eq. (4.1) can be written as

$$\dot{x} = Ax(t) + B\dot{u}(t) + BD\xi(t,x) \tag{4.2}$$

Sliding surface can be defined as $\zeta = \{x = \mathbb{R}^{n}\dot{:}\ \sigma(t) = 0\}$, $\sigma(t)$is a linear switching function which can be defined as

$$\sigma(t) = Gx(t) \tag{4.3}$$

where $G \in \mathbb{R}^{m\times n}$is the design matrix

It is assumed that the square matrix GB is non-singular i.e. det (GB)≠0. Time derivative of the switching function from Eq. (4.3) is considered to analyze the sliding mode associated with the sliding surface.

$$\dot{\sigma}(\mathrm{t}) = G\dot{x}(t) \tag{4.4}$$

Substituting the open loop Eq. (4.2) and (4.4) gives

$$\dot{\sigma}(\mathrm{t}) = G(Ax(t) + Bu(t) + M\xi(t,x)) \tag{4.5}$$

Therefore, for all time, $t > t_s$, it is assumed the all the states are forced to reach the sliding surface and an ideal sliding motion can be obtained. For all $t > t_s$

$$\sigma(\mathrm{t}) = \dot{\sigma}(\mathrm{t}) = 0 \tag{4.6}$$

By equating the time derivative to 0, $u_{eq}(t)$ is obtained. For all $t > t_s$

$$u_{eq}(t) = -(GB)^{-1}\big(GAx(t) + GBD\xi(t,x)\big) \tag{4.7}$$

GB is non-singular. $u_{eq}(t)$ is an equivalent control with an average value that the control signal should maintain to ensure sliding on the sliding surface. In order to achieve sliding motion, substitute Eq. (4.7) into Eq. (4.2) can be written as:

$$\dot{x}(t) = Ax(t) + B\left(-GB)^{-1}\big(GAx(t) + GBD\xi(t,x)\big)\right) + BD\xi(t,x) \tag{4.8}$$

$$I_n - B(GB)^{-1}GAx(t) + (I_n - B(GB)^{-1}G)BD\xi(t,x) \tag{4.9}$$

$$I_n - B(GB)^{-1}G = \Gamma, \tag{4.10}$$

The projection operator holds the property $\Gamma B = 0$

Therefore, Eq. (2.8) reduces to

$$\dot{x}(\mathrm{t}) = \Gamma \mathrm{Ax(t)} for\ t \geq t_s \tag{4.11}$$

From the equation transformation it is clear that during the sliding mode the disturbance has been completely rejected thereby making the system insensitive to the matched uncertainty. The stability of the sliding mode depends on the sliding surface, basically the choice of the switching matrix G.

3.3 Sliding Mode Control Law

After the sliding surface the next task is to define a control law such the sliding motion on the surface is guaranteed. A sliding mode controller typically consist of two parts; a linear part and a non-linear part.

$$u(t) = u_0(t) + u_n(t) \tag{4.12}$$

The non-linear, $u_n(t)$ part is responsible for generating a sliding mode on the surface and the linear part, $u_l(t)$ for helping to maintain sliding. Input u(t) for a multi-variable system can be written as follows:

$$u(t) = -(GB)^{-1}GAx(t) - \rho(t,x)(GB)^{-1}\frac{\sigma(t)}{\|\sigma(t)\|} \tag{4.13}$$

For all $\sigma(t) \neq 0$. $\frac{\sigma(t)}{\|\sigma(t)\|}$, is the unit vector component and $\rho(t,x)$is scalar gain chosen larger than the size of the uncertainty present in the system which will favour sliding motion.

3.4 Reachability

The input u(t) in sliding mode control is designed in such a way that reachability condition is satisfied. Reachability condition is the approach of states towards $\sigma(t) = 0$. The following condition is satisfied to reach the sliding mode.

$$\lim_{\sigma(t)\to 0+} \dot{\sigma}(t) < 0 \text{ and } \lim_{\sigma(t)\to 0-} \dot{\sigma}(t) > 0 \tag{4.14}$$

The equation can be explained by the process by which the derivative of $\dot{\sigma}(t)$ is less than 0, $\sigma(t)$ tends to positive side and when $\dot{\sigma}(t)$ is greater than 0, $\sigma(t)$ tends to negative side. For multi-input system, multivariable version of reachability condition is

$$\sigma^T(t)\dot{\sigma}(t) < -\eta\|\sigma(t)\| \tag{4.15}$$

This condition shows that the sliding condition is attractive.

3.5 Modelling of SMC

Sliding mode control system for quadrotor dynamics was modelled on Simulink. Input u(t) is derived as shown in the previous section. For simplicity, a sine wave is selected as reference trajectory for tracking. Gain K is obtained from LQR as part of linearization process. For waypoint tracking, PID and PD controllers are used for altitude and yaw angle Ψ as shown in figure 10. The desired positions $x_d \; and \; y_d$ are incorporated in the inner loop. A sine wave is used as an external disturbance to analyze the output as shown in figure 11.

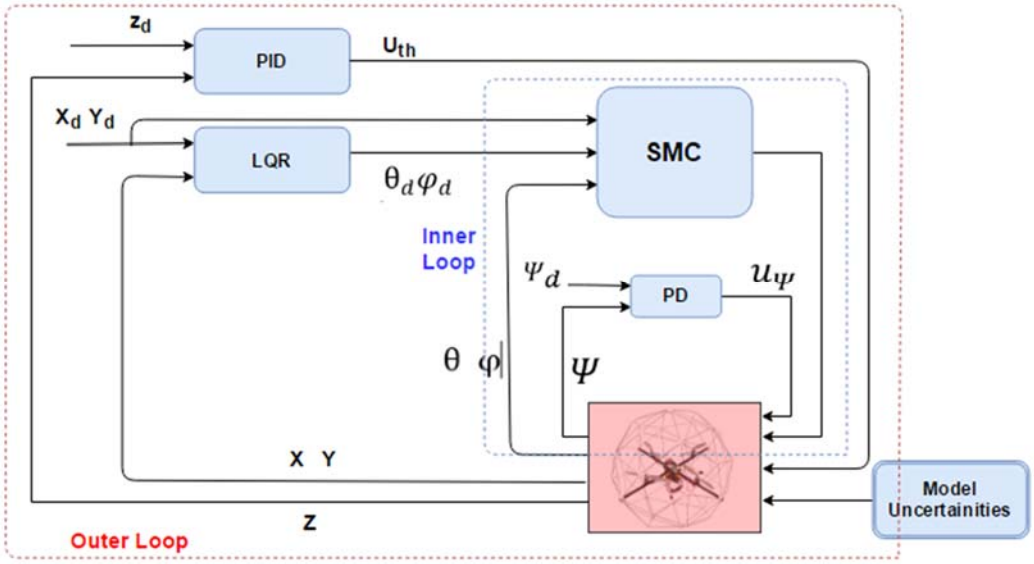

Figure 10: Sliding Mode Control System [5]

Dynamics equations of Quad-rotor in state space form are obtained from the m-file attached in the appendix.

The control system is modelled based on the following equation: [6] [12]

$$u(t) = -(GB)^{-1}GAx(t) - \rho(t,x)(GB)^{-1}\frac{\sigma(t)}{\|\sigma(t)\| + \delta} \quad for \ \sigma(t) \neq 0 \tag{4.16}$$

where $A = \begin{bmatrix} 0 & 1 & 0 & 0 & 0 \\ 0 & 0 & g & 0 & 0 \\ 0 & 0 & 0 & 1 & 0 \\ 0 & 0 & 0 & 0 & \frac{2kl}{J} \\ 0 & 0 & 0 & 0 & -\omega \end{bmatrix}$, $G = [0\ 0\ 0\ 0\ 1]$, $B = [0\ 0\ 0\ 0\ \omega]^T$, $\rho = 0.05$, $\sigma(t) = Gx(t)$

and $\delta = 0.001$

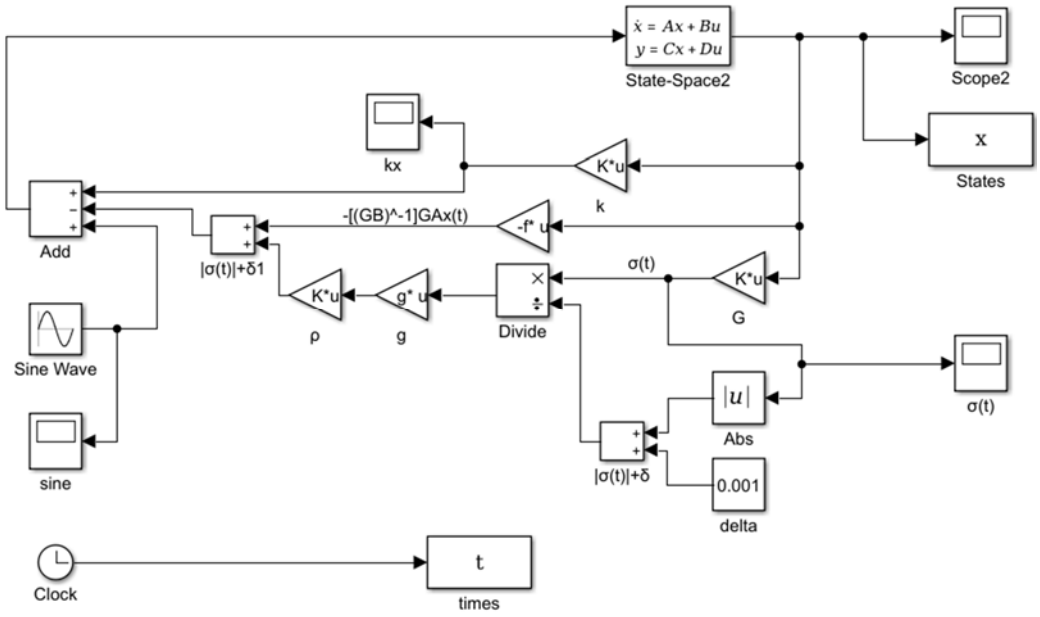

Figure 11: Simulink model of sliding mode controller

SMC system as shown in Figure 14 was modelled based on the mathematical model and dynamics as shown in the previous sections. As mentioned in the section for SMC control law linear input $u_l(t)$ is obtained by using an LQR gain and by modelling non-linear input $u_n(t)$. A sine wave is added as a disturbance to the system. δ is a small positive design scalar added to the signal. G is design matrix and it is assumed that GB is a non-singular matrix. sliding surface $\sigma(t)$ is formed using the dynamics equations as shown in Figure 15.

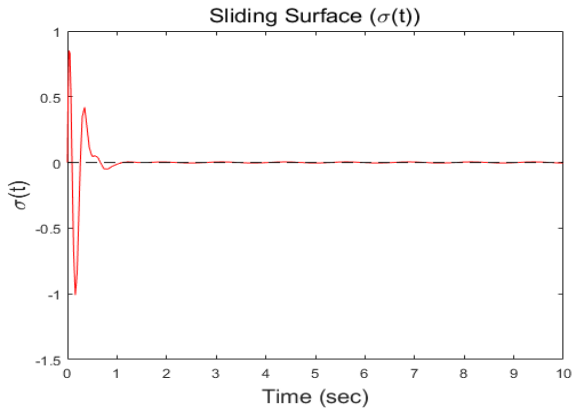

Figure 12: Sliding Surface (σ(t))

The desired states include the position in x-axis, x, velocity in x-axis, $\dot{x}$, angular position, θ , angular velocity, $\dot{\theta}$ and the actuator dynamics, v_θ. Using the gain obtained from LQR and the non-linear control input all the system states asymptotically converges to 0 as shown in section 3.7

Position and velocities are plotted and it shows the sliding mode $\sigma(t)$ exists and all the states approaches the sliding surface. Once on the sliding surface, the switching condition maintains the states to slide along the surface, it is also observed that there are chattering associated with the dynamics. Plots below shows how the five different states approach the sliding surface, $\sigma(t) = 0$. The states are plotted in the ascending order in the state vector given below.

$$\text{State vector } X(t) = \begin{bmatrix} x \\ \dot{x} \\ \theta \\ \dot{\theta} \\ v_\theta \end{bmatrix} \tag{4.17}$$

3.6 Simulation Results

Simulation of Quadrotor dynamics was conducted to analyze the behaviour of the states in various conditions. During initial simulations, it was found that the system exhibits considerable amount of chattering. Following simulation results shows that the chattering can be reduced by tuning the positive constant δ and the step response towards the desired state can be optimized by tuning modulation gain, ρ. The states were also analyzed for system response with starting from different initial conditions. Simulations were conducted several times to optimize the response and reduce chattering. Some of the most critical results are added in this report to show the large variation and to show the improved system states with noticeable change. As part of the optimization process, system analysis was performed based on the following criteria:

Sl. No	Parameters/Initial States	Value Range
1.	Modulation Gain (ρ)	0.05 – 20
2.	Positive Constant (δ)	0.001 – 0.2
3.	Initial States	[-3 0 0 0 0], [0 0 0 0 0]

Table 2: Simulation Procedure for SMC

As shown in Figure 10, a small disturbance was applied to the system using a sine wave. The disturbance was added to the feedback system to observe the system states response in its presence. Figure 14 shows the comparison of state response with LQR and SMC. Analysis is focussed on the overshoot of system state X. In UAV's, the significance of precision in positioning is very important. When the overshoot is closely observed, it is evident that the modulation gain plays an important role in the behaviour of the system state while approaching the desired sliding surface.

Simulations were performed to prove that the sliding mode exist as shown in Figure 11 and the behaviour of the states.

- Simulations with ρ = 0.001 and ρ = 0.5

ρ = 0.001	ρ = 0.5
δ = 0.001	δ = 0.001
Initial State: [-3 0 0 0 0]	Initial State: [-3 0 0 0 0]

Table 3: Simulations with ρ = 0.001 and ρ = 0.5

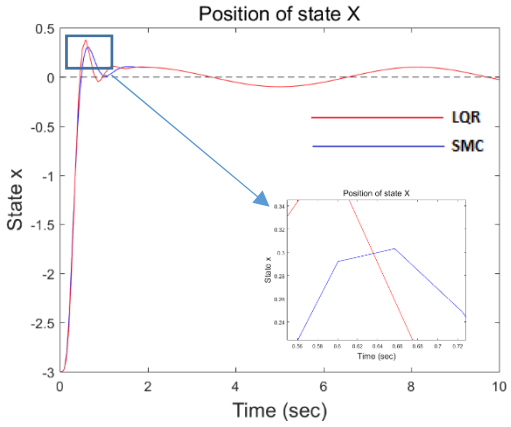

Figure 13: Position of state X with ρ = 0.001

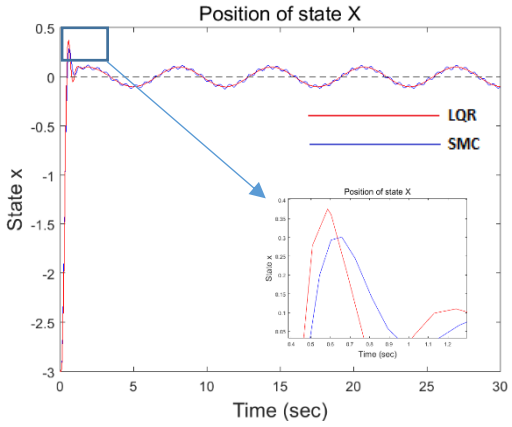

Figure 14: Position of state X with ρ = 0.05

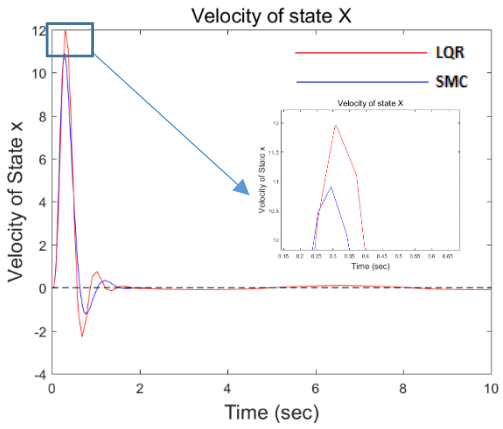

Figure 15: Velocity of state X with ρ = 0.001

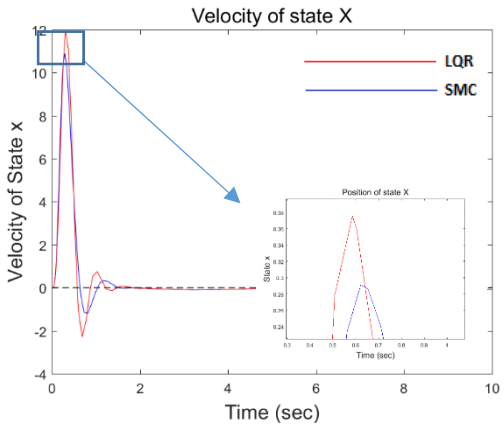

Figure 16: Velocity of state X with ρ = 0.05

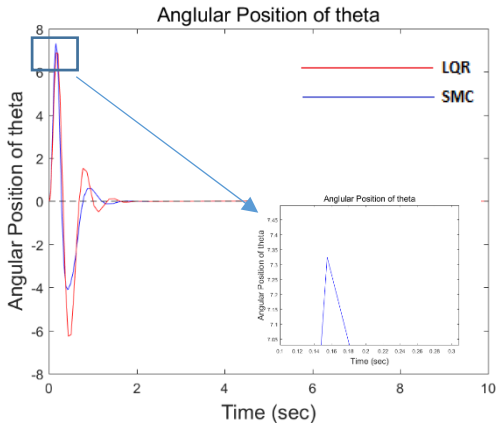

Figure 17: Angular position of θ with $\rho = 0.001$

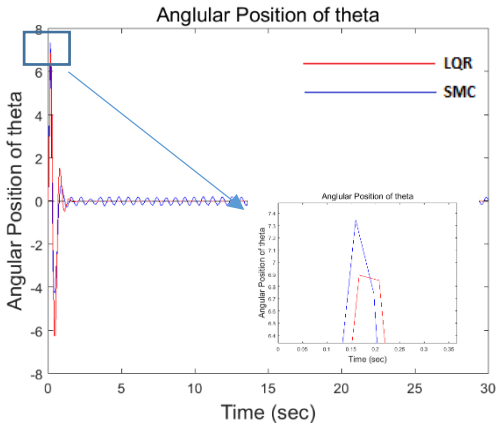

Figure 18: Angular position of θ with $\rho = 0.05$

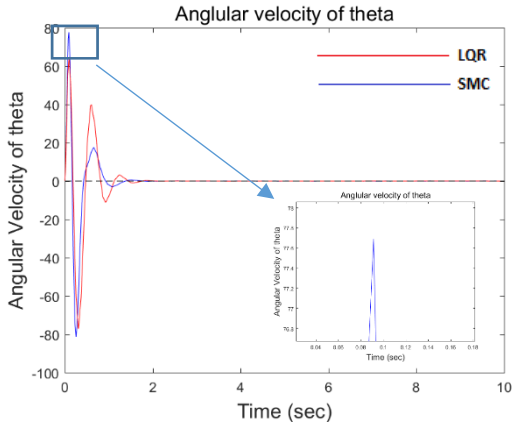

Figure 19: Angular velocity of θ with $\rho = 0.001$

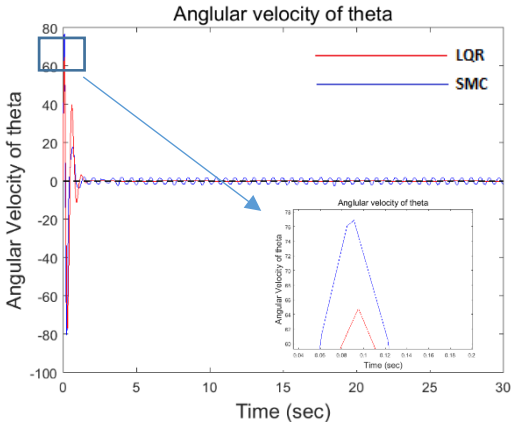

Figure 20: Angular velocity of θ with $\rho = 0.05$

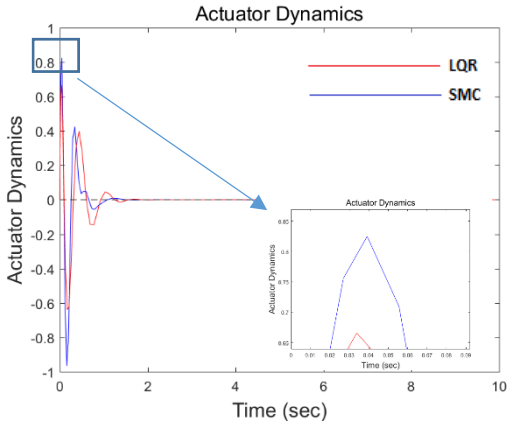

Figure 21: Actuator Dynamics with $\rho = 0.001$

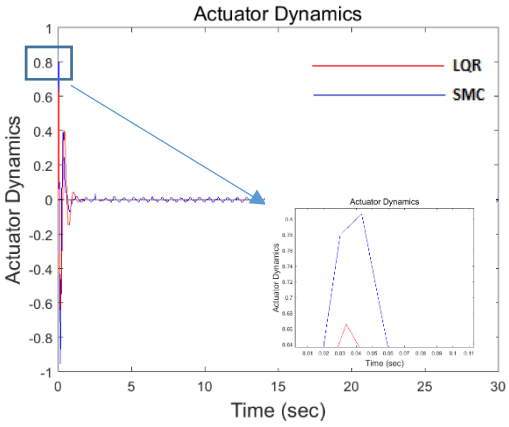

Figure 22: Actuator Dynamics with $\rho = 0.05$

The following simulation is conducted to analyze the systems using different modulation gains as per table 2. The following simulation results show the difference in state behaviour with different modulation gain.

The simulations from Figure 13 to Figure 22 shows the increasing in chattering when modulation gain is increased from $\rho = 0.001$ to $\rho = 0.05$. From Figure 13 and 14, it is clear that chattering has increased with a small reduction of overshoot by using $\rho = 0.05$. From Figure 15 and 16 it is clear that velocity towards position x experience heavy chattering with the use of $\rho = 0.05$, but the settling time is almost the same. Angular position of θ in Figure 17 and 18 shows that SMC reached the desired state faster than LQR even though there is an slight increase overshoot in the beginning. In Figure 19 and 20, overshoot of angular velocity reduces by an amplitude of 2 and reaching a stable condition in less than 1 sec. Actuator dynamics in Figure 21 and 22 maintains the error between the PWM signals for the Quadrotor to move along the x –axis, at the same time the Figure 22 shows heavy dynamics.

3.7 Chattering Reduction

Simulation results showed considerable amount of chattering. Chattering causes excitation of unmodelled system dynamics which may lead to instability. It may also cause high power consumption and possible actuator damage which makes it harder to apply SMC on real systems. [13] Several attempts were made to reduce chattering by trying out different modulation gains, ρ, and value of δ as a positive design scalar. Figure 22 shows the behaviour of chattering. The presence of sgn term in SMC control law makes it discontinuous. The system states is attracted towards sliding surface S=0 in both the conditions where S<0 and S>0 causing the states to slide along the sliding surface. In ideal case, the control law should slide on the surface as soon as it reach the surface. The shift between positive and negative sides of the sliding surface causes chattering. The shifting is caused due to the delay between the change of sign of S and the change in control action.

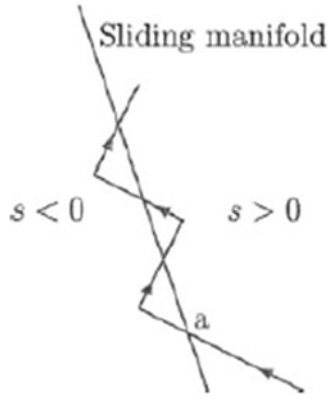

Figure 23: Sliding Mode [9]

As shown Figure 13, 15, 17. 19 and 21, heavy chattering was involved with the system which will damage mechanical components of the system. Further simulations showed reduced chattering reduction as the value of the positive constant δ was increased. Simulations were conducted for a better modulation gain. Modulation gain, ρ = 5 exhibitted improved performance which was selected as a standard value for further simulations. Following Figures 23, 24 and 25 shows chattering reduction at three distinct value for δ = 0.001, δ = 0.09 and δ = 0.1. Finally, positive constant δ = 0.2 and ρ = 5 was selected as optimal values for SMC. Figure simulation results are shown from Figure 26 to 25 provides a comparison between the values δ = 0.001, ρ = 0.001 and δ = 0.2, ρ = 5

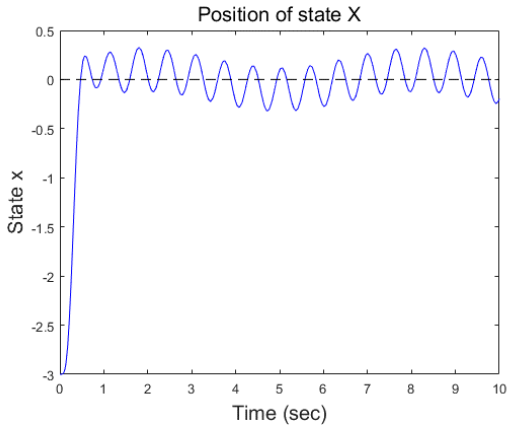

Figure 24: Chattering with ρ = 5 and δ = 0.001

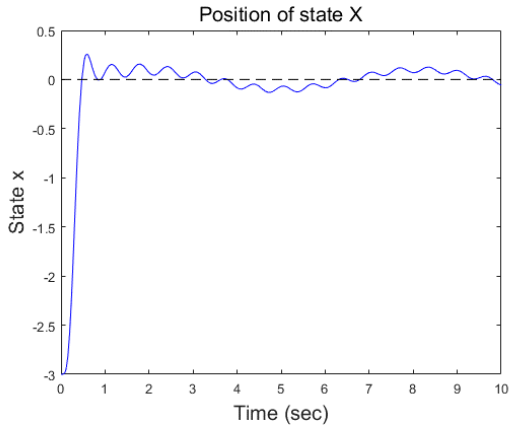

Figure 25: Chattering with ρ = 5 and δ = 0.09

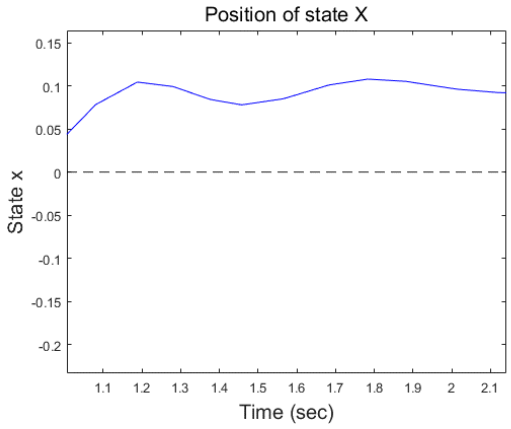

Figure 26: Chattering with ρ = 5 and δ = 0.1

- Simulations with $\rho = 1.3, \delta = 0.001$ and $\rho = 5, \delta = 0.2$

$\rho = 1.3$	$\rho = 5$
$\delta = 0.001$	$\delta = 0.2$
Initial State: [-3 0 0 0 0]	Initial State: [-3 0 0 0 0]

Table 4: Simulations with $\rho = 1.3$, $\delta = 0.001$ and $\rho = 5$, $\delta = 0.2$

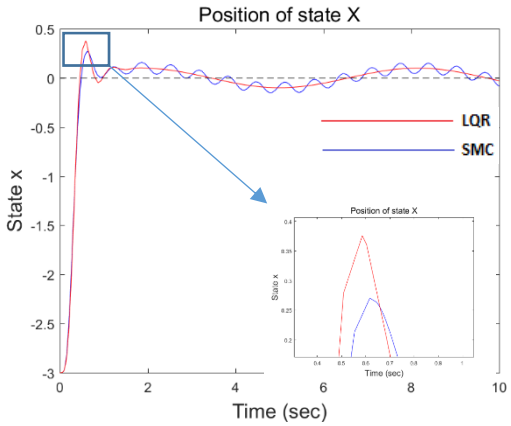

Figure 27: State X with $\rho = 1.3$ and $\delta = 0.001$

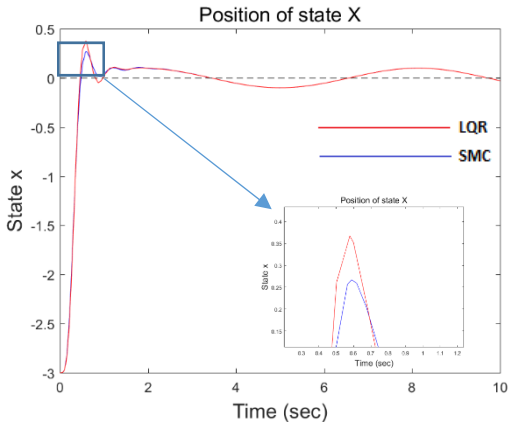

Figure 28: State X with $\rho = 5$ and $\delta = 0.2$

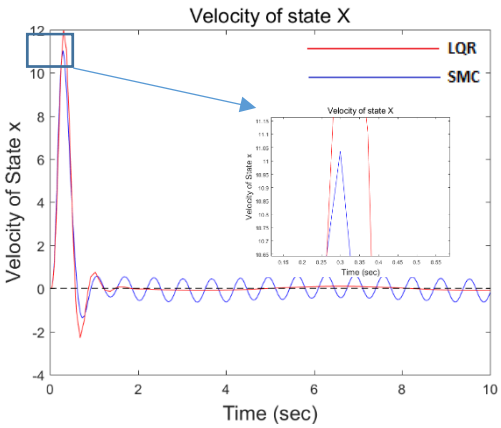

Figure 29: Velocity of state X with $\rho = 1.3$ and $\delta = 0.001$

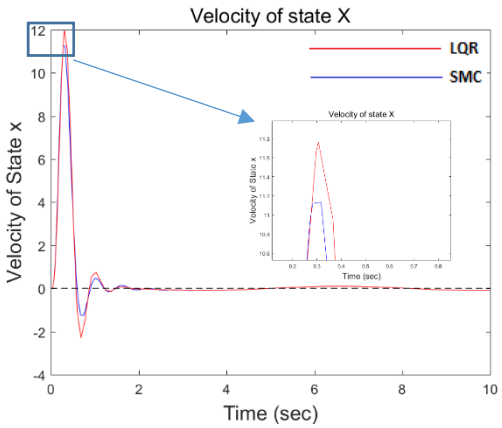

Figure 30: Velocity of state X with $\rho = 5$ and $\delta = 0.2$

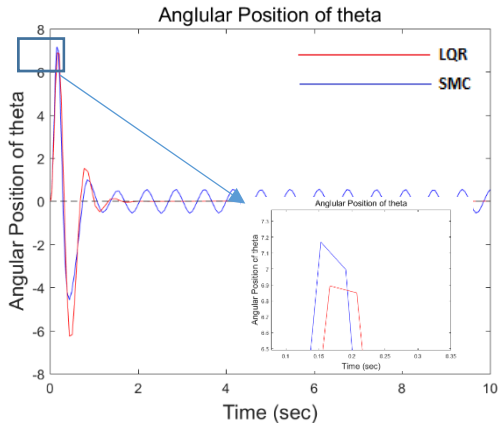

Figure 31: Angular Position of θ with $\rho = 1.3$ and $\delta = 0.001$

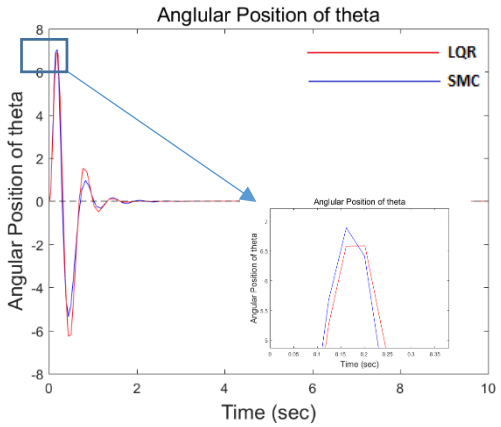

Figure 32: Angular position of θ with $\rho = 5$ and $\delta = 0.2$

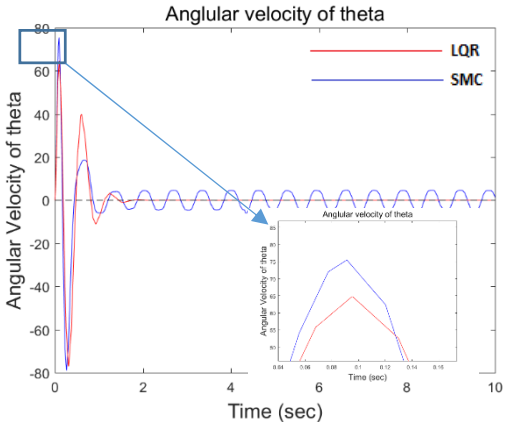

Figure 33: Angular velocity of θ with $\rho = 1.3$ and $\delta = 0.001$

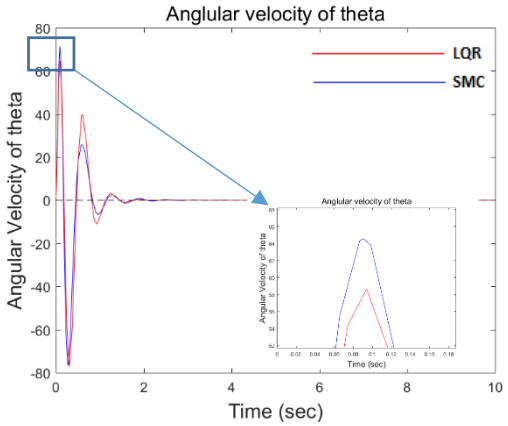

Figure 34: Angular velocity of θ with $\rho = 5$ and $\delta = 0.2$

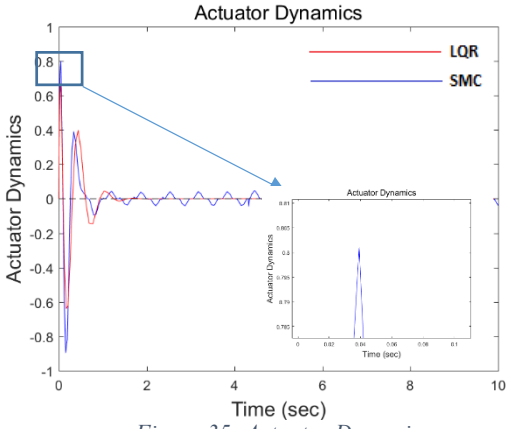

Figure 35: Actuator Dynamics

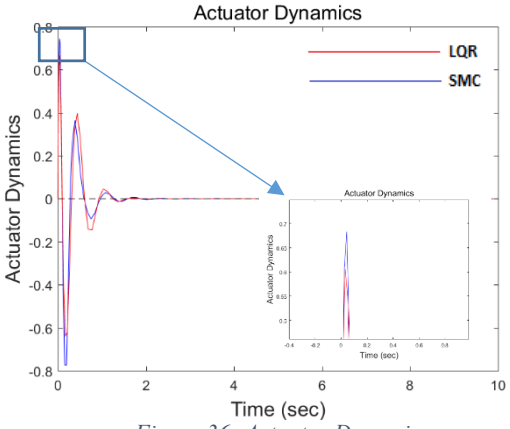

Figure 36: Actuator Dynamics

Above results shows that chattering has drastically reduced. The overshoot has improved from an amplitude of 0.37m to 0.25m while the LQR controller shows an overshoot of 0.37m in position of state x when Figures 26 and 27 are compared.

To verify, more simulations were run to find resulting of values of $\delta = 0.5$ and $\delta = 0.9$ demonstrating improvements than $\delta = 0.05$. These values were selected as there was no considerable difference during the simulations conducted with modulation values until 2.

Therefore values $\delta = 0.2$ and $\rho = 5$ are taken as optimized values for the system. These values are used or further simulations to analyze the effect of initial states on system response and comparison between system response to LQR gain and SMC. It is evident from the following results that system states reach the desired state 0 faster than the states which are offset to 0. It can also be observed that initial excitation of states are very less when compared to previous simulation results when the system is initiated from state [0 0 0 0 0]. The following result shows variation of system response to initial states.

- Simulation with initial states [-3 0 0 0 0] and [0 0 0 0 0]

$\rho = 5$	$\rho = 5$
$\delta = 0.2$	$\delta = 0.2$
Initial State: [-3 0 0 0 0]	Initial State: [0 0 0 0 0]

Table 5: Simulation with initial states [-3 0 0 0 0] and [0 0 0 0 0]

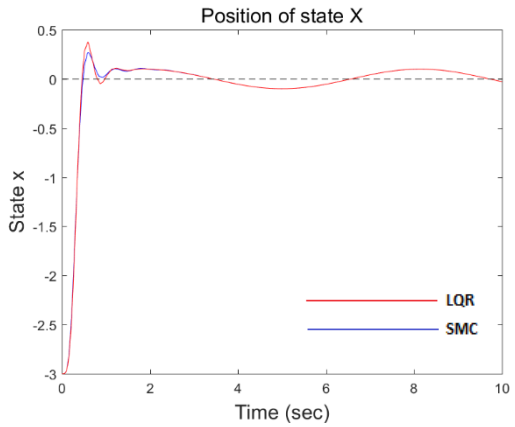

Figure 37: State x with initial state [-3 0 0 0 0]

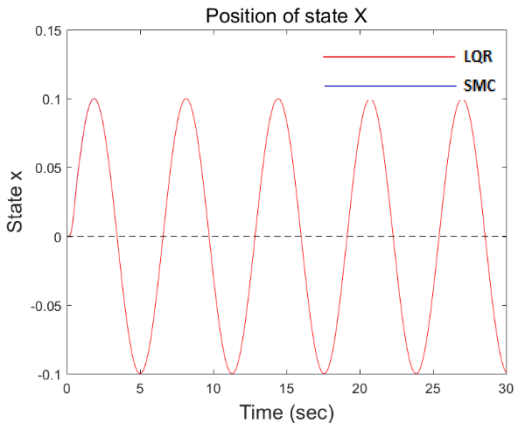

Figure 38: State x with initial state [0 0 0 0 0]

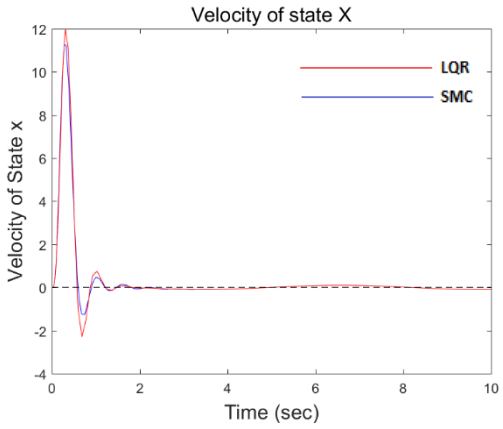

Figure 39: Velocity of state x with initial state [-3 0 0 0 0]

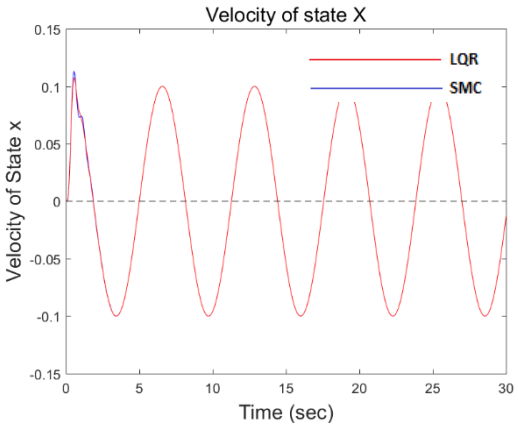

Figure 40: Velocity of state x with initial state [0 0 0 0 0]

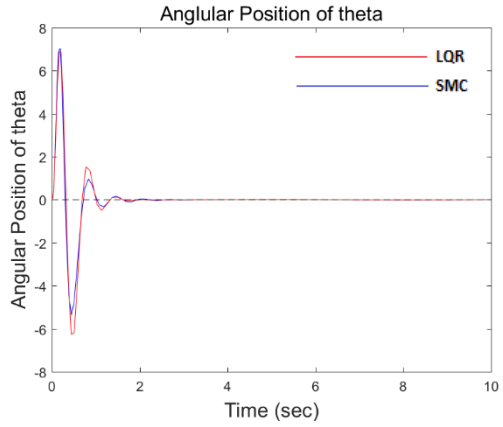

Figure 41: Angular position θ with initial state [-3 0 0 0 0]

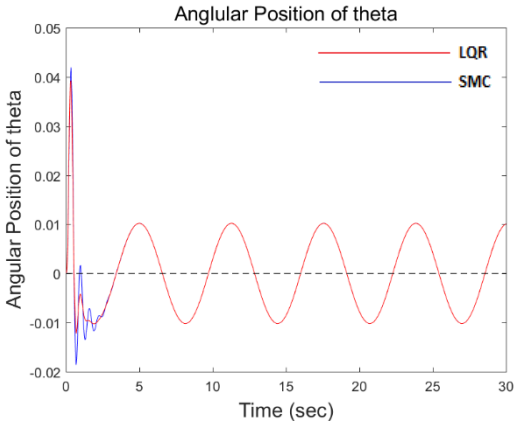

Figure 42:Angular position of θ with initial state [0 0 0 0 0]

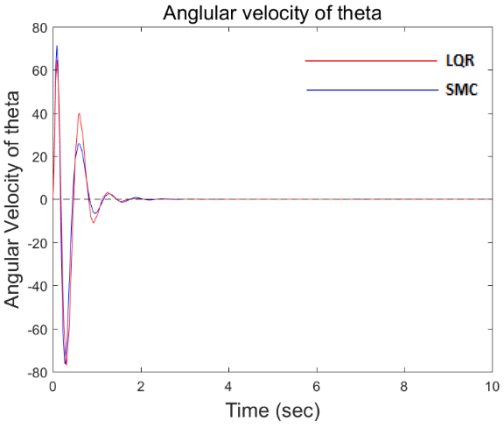

Figure 43: Angular velocity of θ with initial state [-3 0 0 0 0]

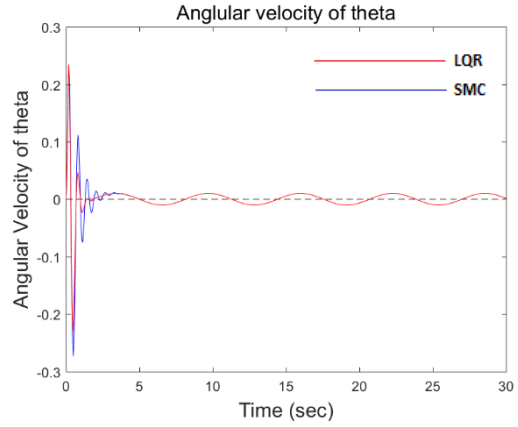

Figure 44: Angular velocity of θ with initial state [0 0 0 0 0]

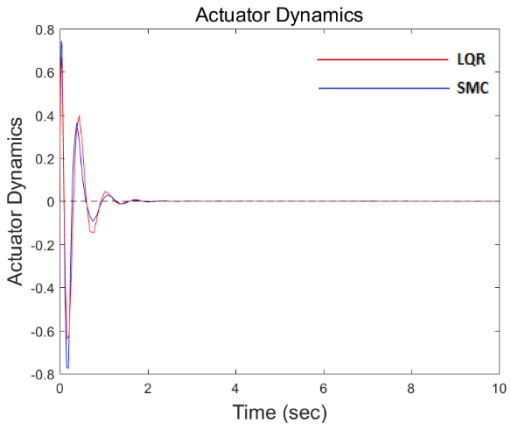

Figure 45: Actuator Dynamics with initial state [-3 0 0 0 0]

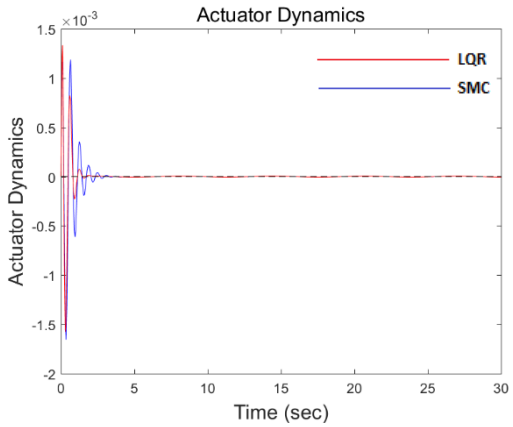

Figure 46: Actuator Dynamics with initial state [0 0 0 0 0]

The Figures 39, 41, 43, 45 and 46 on right hand side shows the simulation results for initial states [0 0 0 0 0]. The simulations were run for 30 seconds to check for consistency. The results show the output of the states maintains a amplitude of 0.1 and frequency of 10. However the results show initial excitation of states in velocity if state X, angular position of θ, velocity of θ and actuator dynamics

3.8 Conclusion

In this chapter, SMC was modelled on Quadrotor dynamics which was derived in Chapter 2. The system was simulated to prove that all the states asymptotically converges to zero. System states were then analysed for ideal behaviour. As part of improvising state response, several simulations were conducted to study the system response to different values of modulation gain. As a result it was found that the performance of state convergence towards the desired value increased as modulation gain increased from 0.01 to 5. The performance was evaluated by closely analyzing the overshoot, settling time and chattering. Presence of heavy chattering was observed during optimization. As part of chattering reduction, a positive constant δ was optimized by simulating values of δ from 0.001 to 0.2. The optimized system was then analyzed for individual state response to a desired initial state selected as 0. As a result of an overall optimization process, the results showed that chattering reduced considerably low and maintained stability around the desired value with an error of 0.1m. The overshoot reduced to an amplitude of 0.25m where LQR exhibited an overshoot of 0.37m in the position state towards X of the system.

Chapter 4

Integral Sliding Mode Controller (ISMC)

4.1 Introduction

Cherna and Wu first proposed Integral Sliding mode control which significantly enhanced robustness against external disturbances of a non-linear system. The system became more efficient in terms of eliminating disturbances and uncertainties [14] However, the robustness against external disturbances and the parameter variations matched to the control can only be achieved after the occurrence of the siding mode. During the reaching phase the system is affected by disturbances and also with the matched uncertainties defined in the system. ISMC was proposed in order to eliminate the reaching phase. Disadvantages and challenges of the system was the strategy affected the performance of the system. Some of the problems were overshoot and response time delay. ISMC is used to enforce a sliding mode from the beginning of a system response. When implementing ISMC, it is assumed that a nominal control system will provide asymptotic stability through the feedback control loop. A discontinuous controller is added to the nominal feedback controller to maintain nominal performance. Bing Xian modelled an ISMC for Quadrotor which will be explained in section 3.6. He used LQR as the gain generator which works as a nominal feedback control system. The following section 3.1 will provide detailed procedure for ISMC synthesis. [12]

4.2 Problem Statement

A linear time invariant system of the following form is considered to explain the procedure for the mathematical model of ISMC

$$\dot{x}(t) = Ax(t) + Bu(t) + M\xi(t,x) + f_u(t,x) \tag{3.1}$$

As explained in the previous chapter is an unknown disturbance and matrix M satisfies the matching condition and can be written as $M = BD$ for some value $D \in \mathbb{R}^{m\times l}$. There is an unmatched uncertainty $f_u(t,x)$ involved in the system which is not in the range space of B. From Eq. (3.1), the nominal linear system can be written in the form

$$\dot{x}(t) = Ax(t) + Bu_0(t) \tag{3.2}$$

Since (A,B) is controllable, state feedback controller is of the form

$$u_0(t) = -Fx(t) \tag{3.3}$$

where $F \in \mathbb{R}^{m \times n}$ is the feedback gain which in this case obtained by using an LQR. The aim of the design procedure is to design an input signal by adding both the nominal feedback control using LQR with ISMC in order to achieve the state $x(t) = x_0(t)$ from the initial time.

4.3 Design Principle

Control law $u(t)$ will be of the form

$$u(t) = u_0(t) + u_n(t) \tag{3.4}$$

where $u_0(t)$ is the nominal controller and $u_n(t)$ is the non-linear controller to induce a sliding mode. Therefore using Eq. (3.4) and (3.1) can be written in the form

$$\dot{x}(t) = Ax(t) + Bu_0(t) + Bu_n(t) + M\xi(t,x) + f_u(t,x) \tag{3.5}$$

$u_n(t)$ will be designed in such a way that it cancels out the matched disturbances term $\xi(t,x)$ while in the sliding mode. The switching function can be defined as

$$\sigma(t) = Gx(t) + z(t) \tag{3.6}$$

where $G \in \mathbb{R}^{m \times n}$, is the switching matrix and can be chosen so that GB is non-singular i.e. $\det(GB) \neq 0$. During sliding, $\sigma(t) = \dot{\sigma}(t) = 0$. Derivative of $\dot{\sigma}(t)$ will be of the form

$$\dot{\sigma}(t) = G\dot{x}(t) + \dot{z}(t) \tag{3.7}$$

In order to achieve the condition were the disturbance $\xi(t,x)$ to be ineffective on the system and if $f_u(t,x) = 0$ and achieve the condition $x(t) = x_0(t)$ for all t>0, substitute equation (3.5) in (3.7)

$$\dot{\sigma}(t) = G(Ax(t) + Bu_0(t) + Bu_n(t) + M\xi(t,x) + f_u(t,x)) + \dot{z}(t) = 0 \tag{3.8}$$

The favourable condition to cover bounded uncertainty is

$$u_{n_{eq}}(t) = -D\xi(t,x) \tag{3.9}$$

Therefore to design a condition that proves the effect of matched uncertainty is completely rejected in the sliding mode $\dot{z}(t)$ can be selected as

$$\dot{z}(t) = -g\big(Ax(t) + Bu_0(t)\big),\ z(0) = -Gx(0) \tag{3.10}$$

which ensures that

$$\dot{\sigma}(t) = GBu_n(t) + GBD\xi(t,x) = 0 \tag{3.11}$$

Therefore by substituting $u_{n_{eq}}$ to equation (3.5) will ensure that the integral sliding mode is governed by the following equation and the condition will also satisfy $x(t) = x_0(t)$ if $f_u(t,x) = 0$ and $x(0) = x_0(0)$

In this case $f_u(t,x) \neq 0$. Therefore, the equivalent control can be substituted in to the switching function

$$u_{n_{eq}}(t) = -(GB)^{-1}GBD\xi(t,x) - (GB)^{-1}Gf_u(t,x) \tag{3.12}$$

$$u_{n_{eq}}(t) = -D\xi(t,x) - (GB)^{-1}Gf_u(t,x) \tag{3.13}$$

Substituting the value $u_{n_{eq}}(t)$ to (3.5)

$$\dot{x}(t) = Ax(t) + Bu_0(t) + (I - B(GB)^{-1}G)f_u(t,x) \tag{3.14}$$

$$(I - B(GB)^{-1}G) = \Gamma \tag{3.15}$$

The equation above shows very clearly that the effect of the matched uncertainty has been rejected while on the sliding mode. However, Γ can amplify the effects of $f_u(t,x)$. By implementing an ISM design parameter G the amplification can be avoided.

4.4 Integral Switching Surface

An integral switching function is selected in such a way that it can eliminate the reaching phase From Eq. (3.6) and (3.10)

$$\sigma(t) = Gx(t) - Gx(0) - \int_0^t Ax(\tau) + Bu_0(\tau))d(\tau) \tag{3.16}$$

By including $Gx(0)$, it is sure that $\sigma(0) = 0$, so that the reaching phase is eliminated and the sliding mode exists from t=0, maintaining system robustness along the closed loop system against the matched uncertainties. G can be selected in such a way that GB is invertible. This condition is enough for ISM design. From [6], it is stated that

$$G = (B^TB)^{-1}B^T \tag{3.17}$$

This particular selection of G in Eq.(3.16) has two advantages

1. The amplitude of chattering can be reduced by minimizing the modulation gain associated with $u_n(t)$ from Eq. (3.4)
2. Avoids the effect of unmatched disturbances.

Simplified property of G can be written as

$$GB = (B^TB)^{-1}B^TB = I_m \tag{3.18}$$

$$(B^TB)^{-1}B^T = G \tag{3.19}$$

The above condition ensures that GB is non-singular and with this choice of G projection operator Γ can be written as

$$\Gamma = I_n - B(B^TB)^{-1}B^T \tag{3.20}$$

Properties of projection operator in Eq. (3.20) is symmetric and idempotent. i.e. $\Gamma^2 = \Gamma$ and $\|\Gamma\| = 1$ which means the effect of $f_u$is not amplified since $\|\Gamma f_u\| \leq \|f_u\|$. It can also be stated that the choice of G is an optimal one for non-amplification and unmatched uncertainty when it proves $\|I - B(GB)^{-1}G\| \geq 1$ for any G

4.5 Integral Sliding Mode Control Laws

As discussed in the introduction, ISM is controlled by a nominal system $u_0(t)$ in Eq. (3.2). The control law has a structure given by Eq. (3.4). $u_n(t)$ is the discontinuous part to enforce a sliding mode along the sliding surface. A choice of $u(t)$ is

$$u(t) = -Fx(t) - \rho(t,x) - (GB)^{-1}\frac{\sigma(t)}{\|\sigma(t)\|} \text{ for } \sigma(t) \neq 0 \tag{3.21}$$

F is the state feedback controller for the performance and $\rho(t,x)$ is the modulation gain to enforce the sliding mode.

4.6 Reachability Condition

To satisfy control input Eq. (3.21) controller satisfies the reachability η to satisfy sufficient condition for sliding motion. From Eq. (3.1) and (3.3)

$$\dot{\sigma}(t) = G\big(Ax(t) + Bu(t) + BD\xi(t,x) + f_u(t,x)\big) - GAx(t) + GBFx(t) \tag{3.22}$$

From Eq. (3.21), Simplified model will be

$$\dot{\sigma}(t) = GAx(t) + GB(-Fx(t) + u_n(t)) + GBD\xi(.) + Gf_u(.) - GAx(t) + GBFx(t) \tag{3.23}$$

$$\dot{\sigma}(t) = -\rho(t,x)\frac{\sigma(t)}{\|\sigma(t)\|} + GBD\xi(t,x) + Gf_u(t,x) \tag{3.24}$$

To prove reachability condition,

$$\dot{\sigma}(t)\sigma^T(t) = -\rho(t,x)\|\sigma(t)\| + \sigma^T(t)D\xi(t,x) + \sigma^T(t)Gf_u(t,x) \tag{3.25}$$

$$\dot{\sigma}(t)\sigma^T(t) \leq \|\sigma^T(t)\|(-\rho(t,x) + \|D\xi(t,x)\| + \|Gf_u(t,x)\| + \eta \tag{3.26}$$

η is a positive scalar

$$\sigma^T(t)\dot{\sigma}(t) \leq -\eta\|\sigma(t)\| \tag{3.27}$$

Therefore the reachability is satisfied.

The reachability condition can also be verified by Lyapunov theory. Lyapunov candidate can be selected as $V(t) = \frac{1}{2}\sigma(t)\sigma^T(t)$ and $\dot{V}(t) = \dot{\sigma}(t)\sigma^T(t)$. From the above equations it is clear that

$$\dot{V}(t) \leq -\eta\|\sigma(t)\| = -\eta\sqrt{2V(t)} \tag{3.28}$$

By integrating on both the sides

$$\sqrt{2V(t)} - \sqrt{2V(0)} \leq -\eta t \tag{3.28}$$

It shows that $V(t) = 0$ is less than $\frac{n}{\sqrt{2V(0)}}$ units of time

4.7 Modelling of ISMC

In sliding mode control, a reaching phase exists where the states approach the desired states. This event is eliminated by using Integral Sliding mode control and the system starts in a predetermined sliding mode by achieving robustness throughout the entire system response. ISMC has been applied to quadrotor for control of 3-DOF in [13]. Bing Xian with Dr. Yang Shi. [6] designed and implemented ISMC on quadrotor based on the system dynamics as shown in Chapter 1. As part of this project ISMC was simulated for optimal values of modulation gain which can cancel the external disturbance as shown in section 4.8. As shown in Eq. 3.16, the actual state Gx(t) is subtracted form Gx(0) which represent the desired dynamics.

Properties of Sliding mode can be identified as follows:

- No reaching phase and the sliding mode is enforced throughout the system response.
- During sliding order of motion is same as that of the original system
- The effect of unmatched uncertainty can be mitigated by designing a suitable sliding surface
- System motion will be invariant to matched uncertainty during the sliding mode
- ISMC can also be combined with an existing feedback system

The main contributions of the work are as follows: [6]

- ISMC is applied on 6-DOF Quadrotor flight control incorporating the reference signal angles and the desired position information and stability of the system is analyzed using Lyapunov approach.
- An LQR and ISMC based control system was proposed on a commercially available quadrotor. The performance of the controllers are compared in terms of Mean Square Error (MSE). Experimental comparisons were conducted by enlarging the model uncertainties and external disturbances by attaching an unknown weight to the quadrotor.

ISMC is designed for waypoint tracking in the presence of both model uncertainties and external disturbances. As shown in figure 10, PID and PD controllers are used for altitude and yaw angle Ψ. Therefore they are considered for controller design. The desired positions $x_d \; and \; y_d$ are incorporated in the inner loop as shown in figure. Since the dynamics of the quadrotor along x and y axis are decoupled and similar, ISMC based controller is proposed only along x axis.

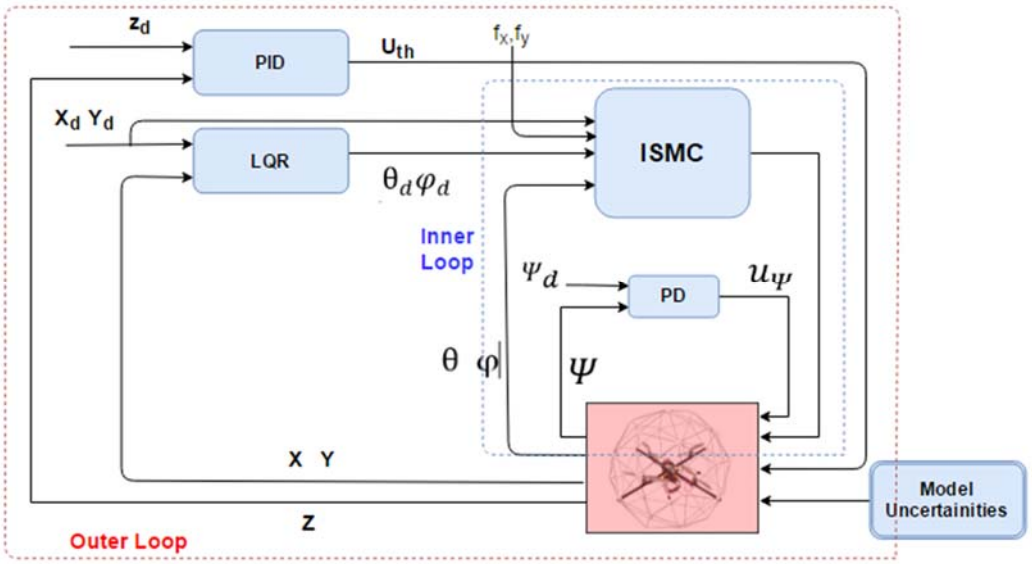

Figure 47: ISMC Control loop [6]

ISMC is implemented in Simulink to compare results with the experimental results. The system is modelled using the following control input $u_\theta(t)$ as formulated in previous section 4.6

$$u_\theta(t) = -Fx(t) - \rho(t)(GB_x)^{-1}\frac{\sigma_x(t)}{\|\sigma_x(t)\| + \delta} \tag{3.28}$$

where $\delta = 0.0001$ is a small scalar to eliminate chattering and $x(t) = \begin{bmatrix} x \\ \dot{x} \\ \theta \\ \dot{\theta} \\ v_\theta \end{bmatrix}$ is the state vector

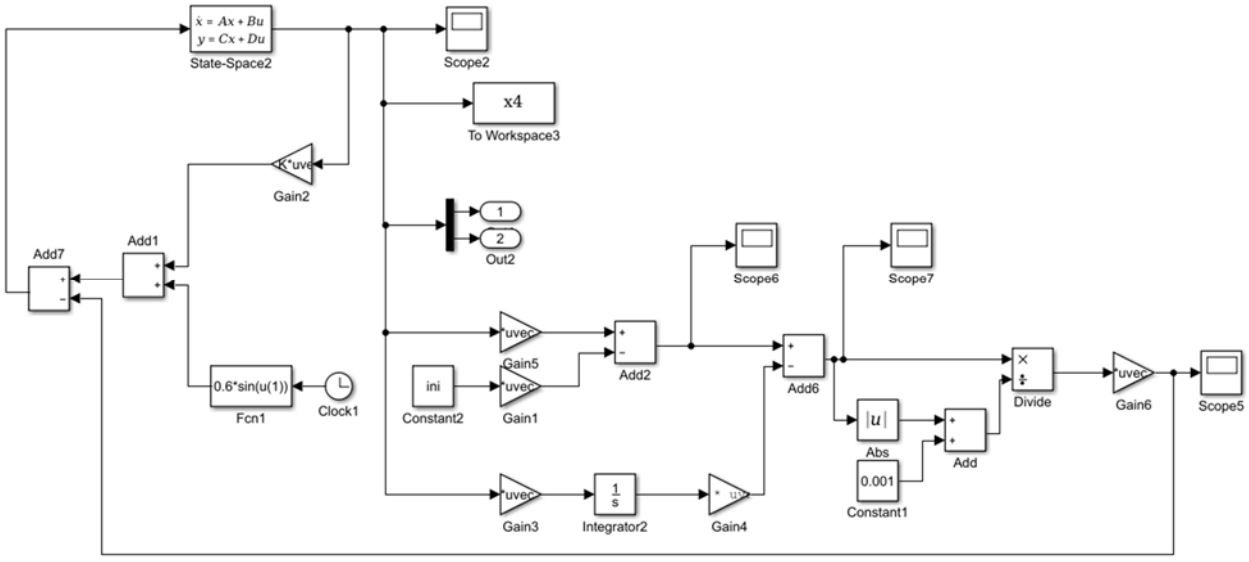

Figure 48: ISMC Control System Model

Linearization procedure of Quadrotor had inevitable variations in results as a result of neglecting intrinsic feature of non-linearities in dynamics and excluding centrifugal force, centripetal force and drag forces. Tests were conducted in two conditions of the system. First set was application LQR and ISMC based controller to quadrotor to conduct waypoint tracking. Secondly, repeating the same experiment with an added weight of 0.17kg which is unknown to the controller. The weight is attached to the protective cage of Qball. Due to the extra mass, the center of gravity and the momentum of inertia of the B-frame changes. Extra torques are generated by the motors by recalculating the torque required to balance the system stability to compensate the external mass added which is not defined by the system. The experiment is conducted by moving the quadrotor from one point to the other. Data is recorded from the point where the command is sent to target vehicle. The quadrotor moves from the initial point $[x_0 \quad y_0 \quad z_0]^T$ to desired point $[x_d \quad y_d \quad z_d]^T$ with large fluctuation in states with large overshoots and oscillations for several seconds. Experimental results were also compared with LQR using Mean Square Error (MSE) method using the following equation.

$$MSE = \frac{1}{N}\sum_{k=1}^{N}(x(t) - x_d)^2$$

x_d - Desired value

$N -$ Number of sampling during the waypoint tracking

Case	a	b	c	d
X	0.1855	0.1455	0.3071	0.1666
Y	0.1457	0.1123	0.2165	0.1125
θ	0.0026	0.0020	0.0090	0.0047
φ	0.0023	0.0018	0.0054	0.0040

Table 6: MSE results for LQR and ISMC [6]

Case a: No weight, LQR

Case b: No weight, ISMC

Case c: Additional weight, LQR

Case d: Additional weight, ISMC

The results shows that MSE's of x, y, θ, φ are decreased by using the designed ISMC-based controller.

4.8 Simulation Results

ISMC model was simulated again to analyze and to observe the variation in system response. The following figure shows the existence of the sliding surface, $\sigma(t)$.

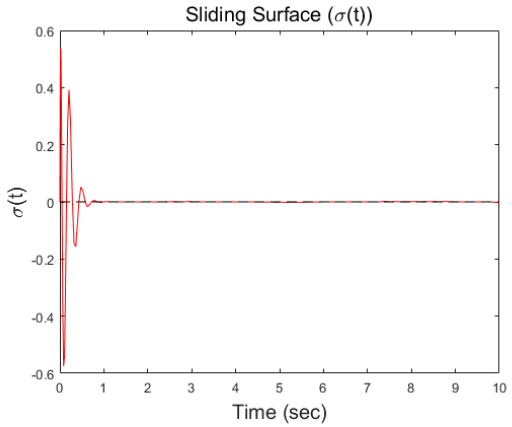

Figure 49: Sliding Surface of ISMC (σ(t))

Simulation was conducted to observe how the states converge to sliding surface, S=0. The following simulation result is comparison of system state response to LQR and ISMC.

The states are plotted in the ascending order in the state vector given below.

$$\text{State vector } X(t) = \begin{bmatrix} x \\ \dot{x} \\ \theta \\ \dot{\theta} \\ v_\theta \end{bmatrix} \tag{3.29}$$

Initially when the system was the system states converged as shown in left hand side of the following simulation results where LQR and ISMC exhibited almost the same system response. Therefore modulation gain ρ and the positive constant δ was optimized to analyze system state response. Simulations were conducted based on the following criteria.

Sl. No	Parameters/Initial States	Value Range
1.	Modulation Gain (ρ)	0.01 – 2
2.	Positive Constant (δ)	0.001 – 1.2

Table 7: Simulation procedure for ISMC

- Simulations using $\rho = 0.001$, $\delta = 0.001$ and $\rho = 1.9$, $\delta = 1.2$

$\rho = 0.001$	$\rho = 1.9$
$\delta = 0.001$	$\delta = 1.2$
Initial State: [5 0 0 0 0]	Initial State: [5 0 0 0 0]

Table 8: Simulations using $\rho = 0.001$, $\delta = 0.001$ and $\rho = 1.9$, $\delta = 1.2$

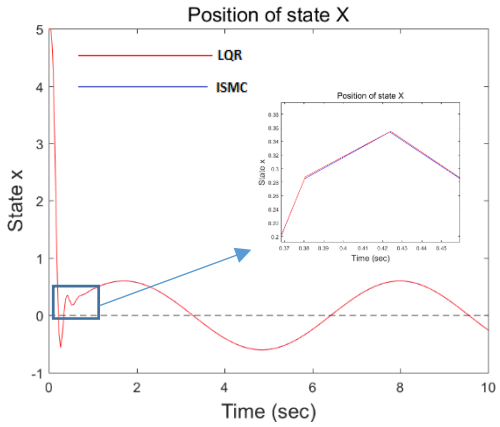

Figure 50: Position of state X with $\rho = 0.001$ and $\delta = 0.001$

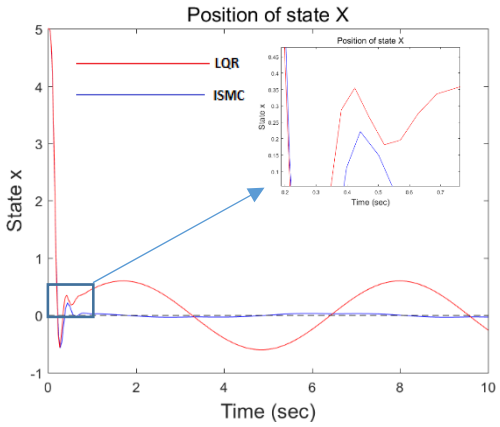

Figure 51: Position of state X with $\rho = 1.9$ and $\delta = 1.2$

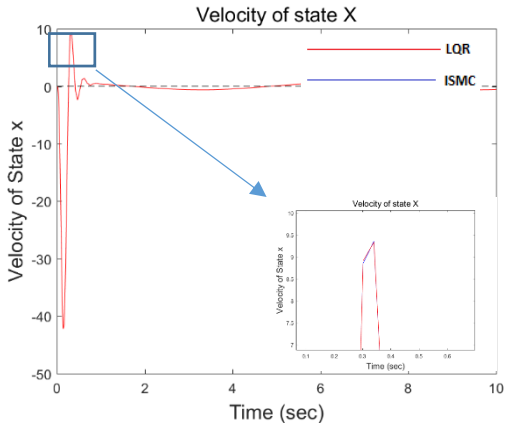

Figure 52: Velocity of state X with $\rho = 0.001$ and $\delta = 0.001$

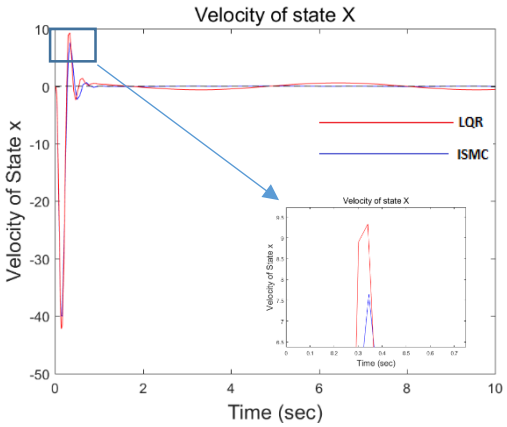

Figure 53: Velocity of state X with $\rho = 1.9$ and $\delta = 1.2$

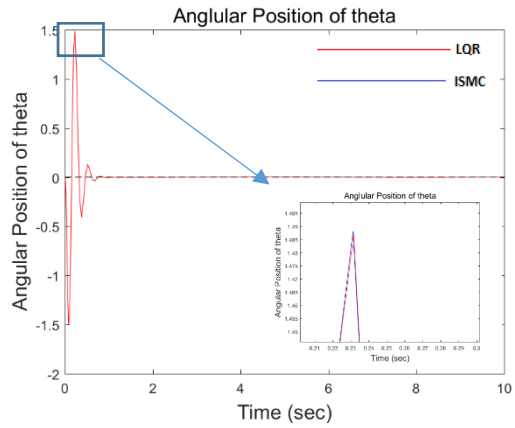

Figure 54: Angular position $\rho = 0.001$ and $\delta = 0.001$

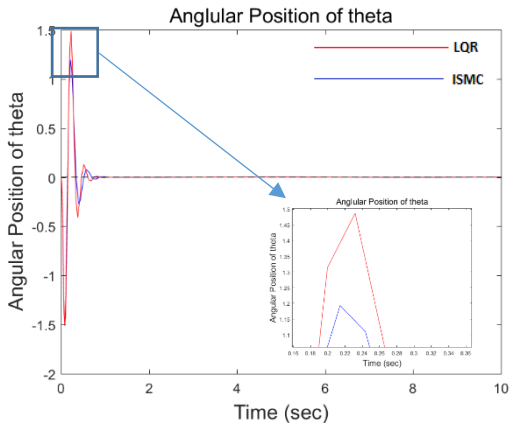

Figure 55: Angular Positon with $\rho = 1.9$ and $\delta = 1.2$

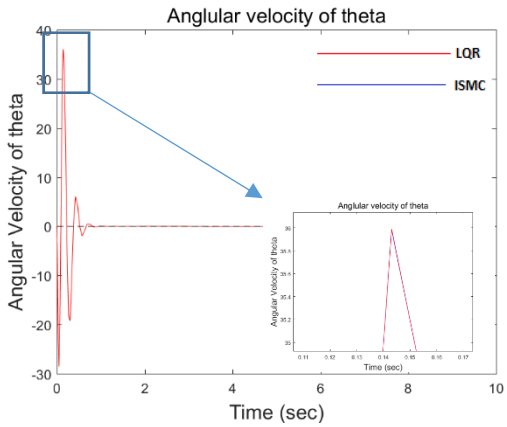

Figure 56: Angular velocity ρ = 0.001 and δ = 0.001

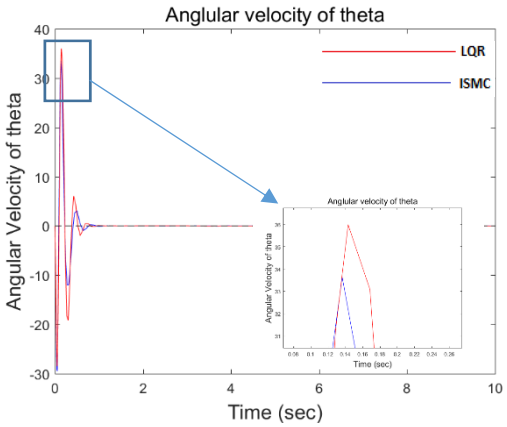

Figure 57: Angular Velocity with ρ = 1.9 and δ = 1.2

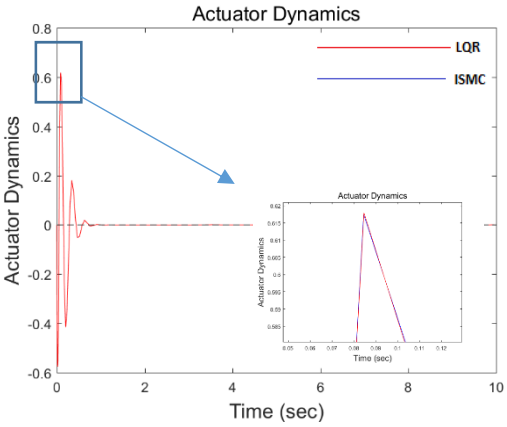

Figure 58: Actuator Dynamics ρ = 0.001 and δ = 0.001

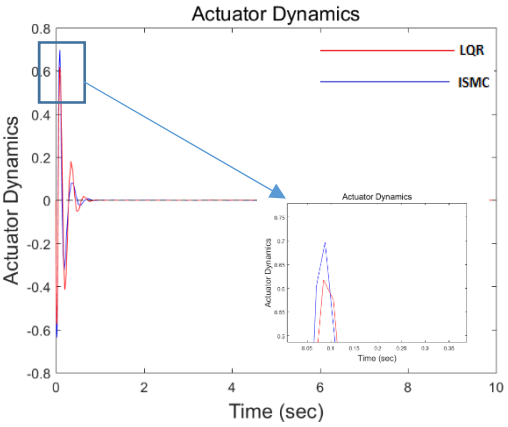

Figure 59: Actuator Dynamics with ρ = 1.9 and δ = 1.2

Figure 49 and 50 shows the position of state X. Simulation using modulation gain ρ = 0.001 and δ = 0.001 shows that the states response is equal to LQR which is not ideal for ISMC. Several simulations were conducted to improve state response using ISMC based on the simulation procedure as shown in table 3. The magnified image shows that the overshoot has reduced to an amplitude of 0.25m from 0.3m with a modulation gain of ρ = 1.9 and δ = 1.2 to control chattering. The optimized values also cancelled the small disturbance added to system as shown in Figure 47. Al the other states of the system stabilizes to the desired value with an initial excitation which lasts only for 0.1 sec as shown in Figure 52, 54, 56 and 58.

4.9 Conclusion

Chapter 4 introduces ISMC for quadrotor which was designed and tested on Qball X4 quadrotor by BingXian. Simulations were conducted in the existing ISMC model to study the properties of ISMC. A matching uncertainty is defined in the system dynamics to cancel out its effect on the

system performance. The reachability condition cancelled in ISMC unlike SMC to start the system on a desired sliding surface. ISMC is validated with experimental results as shown in Table 6 where MSE calculations using ISMC were less than that of LQR.

Simulations were conducted using ISMC based on the simplified quadrotor dynamics using simulation procedures shown in table 6. The results were improved using optimized modulation gain values of $\rho = 1.9$ and $\delta = 1.2$ where the system performance increases when compared to system condition based on $\rho = 0.001$ and $\delta = 0.001$ as shown in the Figure 49 to 58. Chattering was also reduced by finding an optimum value $\delta = 1.2$ after several simulations conducted for values of $\delta = 0.01$ to $\delta = 1.2$.

Chapter 5

5 Conclusion and Future Works

5.1 Conclusion

Sliding mode was implemented on quadrotor dynamics to analyze the system state response and observe that the states converges to the sliding surface and stays on the sliding surface. The presence of chattering was observed. Several simulations were conducted as part of optimization process. Modulation gain and a positive constant included in the modelling of SMC controller was studied to reduce the chattering involved in the system which showed drastic improvement in chattering reduction. Results provided in section 4.4 are simulations conducted on various aspects such as optimization modulation gain, positive constant, δ. Initial condition of states were changed for analysis and performance of LQR and SMC controller were also observed. Quadrotor dynamics were obtained from Qball X4 manufacturer's manual. The project was by completed by studying the work of BingXian, Integral Sliding Mode Control of a Quadrotor in the Presence of Model Uncertainties and External Disturbances in which he designed and implemented ISMC to quadrotor dynamics. Kunwu Zhang's work Flight control of Quadrotor: Theory and Experiments [14] was studied to understand the modelling of Quadrotor.

5.1.1 Advantage and Disadvantages

- **Advantages**
  - ✓ A systematic approach to the problem of maintaining stability and consistent performance in during the effect of modelling uncertainties.
  - ✓ Capable of stabilizing some of the non-linear systems which is not practical using a continuous state feedback system
  - ✓ Achievement of bounded parameter variation and disturbances as soon as the states reach the sliding surface.
- **Disadvantages**
  - ✓ Due to heavy chattering, actuators in a real system are at risk of damage or premature wear as a result of high frequency control actions.
  - ✓ High frequency of control actions may also lead to high power consumption

5.2 Future Works

As part of the future work, SMC can be applied on the test bench (Qball X4 Quadrotor) to analyze the performance as the simulations results and experimental results always differ based on the assumptions made to model the controller. Adaptive Sliding Mode Controller (ASMC) was studied and derived as part of this project. It is very useful to implement the system into quadrotor as it will reject the unmatched uncertainties in theory by estimating and generating an optimal control input to stabilize the system states. The controller can be modelled, simulated and experimented as a future work.

Bibliography

[1] General Atomics Aeronautical, http://www.ga-asi.com/mq-9b "General Atomics MQ-9 Reaper".

[2] A. Zulu and S. John, "A Review of Control Algorithms for Autonomous Quadrotors," *Open Journal of Applied Sciences,* Vols. 547-556, p. 4, 2014.

[3] L. Li, L. sun and J. Jin, "Survey of Advances in Control Algorithms of Quadrotor Unmanned Aerial Vehicle," in *IEEE*, 2015.

[4] Parrot, https://www.parrot.com/ca/drones/parrot-ardrone-20-elite-edition#parrot-ardrone-20-elite-edition "Parrot AR Drone".

[5] K. Zhang, "Flight Control of a Quadrotor: Theory and Experiments," University of Victoria, 2016.

[6] B. Mu and Y. Shi, "Integral Sliding Mode Control for a Quadrotor in the Presence of Model Uncertainties and External Disturbances," 2017.

[7] Quanser Innovate Educate, "Quanser Qball - X4 User Manual".

[8] Quanser Innovate Educate, "Multi Vehicle Co-ordination User Manual," Markham, Ontario., 2012.

[9] A.Gibiansky and http://andrew.gibiansky.com/blog/physics/quadcopter-dynamics/, "Quadrotor Dynamics and Simulation," 2012.

[10] H. Bolandi, M. Rezaei, R. Mosenipour, H. Nemati and S. Smailzadeh, "Attitude control of a Quadrotor with Qptimized PID Controller," *Intelligent Control and Automation,* vol. 4, pp. 335-342, 2013.

[11] D. Mellinger, "Trajectory Generation and Control for Quadrotors," University of Pennsylvania, 2012.

[12] M. Hamayun, C. Edwards and H. Alwi, Fault Tolerant Control Schemes using Integral Sliding Modes, 2016.

[13] H. Nabil, "Dynamic Modeling and Control of a Quadrotor Using Linear and Nonlinear Approaches," Master of Science in Robotics, Control and Smart Systems, The American University of Cairo, 2014.

[14] X. Zheng, X. Jian, D. Wenzheng and C. Hongjie, "Nonlinear Integral Sliding Mode Control for a Second Order Nonlinear System," *Journal of Control Science and Engineering,* pp. Article ID 218198, 7 pages, 2015.

[15] M. Arielle, "A Model-Free Control Algorithm Derived Using the Sliding Model Control Method," Kate Gleason College of Engineering, 2015.

[16] K. Runcharoon and V. Srichatrapimuk, "Sliding Mode Control of Quadrotor," in *Technological Advances in Electrical, Electronics and Computer Engineering (TAEECE)*, 2013.

[17] N. AMMAR, S. BOUALL`EGUE and J. HAGG`EGE, "Modeling and Sliding Mode Control of a Quadrotor Unmanned Aerial Vehicle," *Automation, Control, Engineering and Computer Science (ACECS),* pp. 834-840, 2016.

[18] M. Efe, "Integral sliding mode control of a quadrotor with fractional order reaching dynamics," *Transactions of the Institute of Measurement and Control,* vol. 8, p. 985–1003, 2011.

[19] S. Raza and W. Gueaieb, Intelligent Flight Control of an Autonomous Quadrotor, 2010.

[20] A. Bhatti, "Advanced Sliding Mode Controllers for Industrial Application," University of Leicester, 1997.

[21] A. Bhatti, "Advanced Sliding Mode Controllers for industrial Applications," Department of Engineering, University of Leicester, 1977.

[22] C. Balas, "Modelling and Linear Control of Quadrotor," Cranfield University, 2007.

[23] J. Liu and X. Wang, Advanced Sliding Mode Control for Mechanical Systems, Tsinghua University Press, 2011.

[24] J. Slotine and W. Li, Applied Non-Linear Control, Prentice-Hall Inc., 1991.

[25] B. Bandyopadhayay, J. S and S. Spurgeon, Advances in Sliding Mode Control, Springer Heidelberg New York Dordrecht London, 2013.

A. Appendix

A.1 m.code for Sliding Mode Controller

```
clear;
k=120;
w=15;
J=0.03;
M=1.4;
L=0.2;
Q=diag([1 0 0 0 0]);
R=1;

A2=[0 1 0 0 0;0 0 9.8,0,0;0 0 0 1 0;0 0 0 0 2*k*L/J;0 0 0 0 -w];
B2=[0;0;0;0;w];
C=diag([1 1 1 1 1]);
D=zeros(5,1);
K,S,e]=lqr(A2,B2,Q,R);
F=K;
A2-B2*F
G=[0 0 0 0 1];
f=-inv(G*B2)*G*A2;
ini2=[-3 0 0 0 0]';
ini=[10;-0.4];
g=inv(G*B2);
```

A.2 m.code for Integral Sliding Mode Controller

```
clear;
k=120;
w=15;
J=0.03;
M=1.4;
L=0.2;
Q=diag([1 0 0 0 0]);
R=1;

A2=[0 1 0 0 0;0 0 4*k/M,0,0;0 0 0 1 0;0 0 0 0 2*k*L/J;0 0 0 0 -w];
B2=[0;0;0;0;w];
C=diag([1 1 1 1 1]);
D=zeros(5,1);
[K,S,e]=lqr(A2,B2,Q,R);
F=K;
A2-B2*F
G=inv(B2'*B2)*B2';
H=A2-B2*[0.999,0.135,3.160,0.132,4.403];
f=-inv(G*B2)*0.4;
ini2=[5 0 0 0 0]';
ini=[0;0;0;0;0];
```

A.3 Plot generation for SMC

```
xp1=x(:,1);
xp2=x(:,2);
xp3=x(:,3);
xp4=x(:,4);
xp5=x(:,5);

figure(1)
plot(t,xp1,'blue')
hline = refline(0,0.);
     set(hline,'color','black');
     set(hline,'LineStyle','- -');
title('Position of state X','fontweight','normal','fontsize',15)
ylabel('State x','fontsize',15)
xlabel('Time (sec)','fontsize',15)
hold on;

figure(2)
plot(t,xp2,'blue')
hline = refline(0,0.);
     set(hline,'color','black');
     set(hline,'LineStyle','- -');
title('Velocity of state X','fontweight','normal','fontsize',15)
ylabel('Velocity of State x','fontsize',15)
xlabel('Time (sec)','fontsize',15)

hold on;

figure(3)
plot(t,xp3,'blue')
hline = refline(0,0.);
     set(hline,'color','black');
     set(hline,'LineStyle','- -');
title('Anglular Position of
theta','fontweight','normal','fontsize',15)
ylabel('Angular Position of theta','fontsize',15)
xlabel('Time (sec)','fontsize',15)

hold on;

figure(4)
plot(t,xp4,'blue')
hline = refline(0,0.);
     set(hline,'color','black');
     set(hline,'LineStyle','- -');
title('Anglular velocity of
theta','fontweight','normal','fontsize',15)
ylabel('Angular Velocity of theta','fontsize',15)
xlabel('Time (sec)','fontsize',15)
```

```
hold on;

figure(5)
plot(t,xp5,'blue')
hline = refline(0,0.);
     set(hline,'color','black');
     set(hline,'LineStyle','- -');
title('Actuator Dynamics','fontweight','normal','fontsize',15)
ylabel('Actuator Dynamics','fontsize',15)
xlabel('Time (sec)','fontsize',15)

hold on;

%Sliding Surface-----------------------------------------------------

X1p1=X1(:,1);
plot(t,X1p1,'red');
hline = refline(0,0.);
set(hline,'color','black');
set(hline,'LineStyle','- -');
title('Sliding Surface
(\sigma(t))','fontweight','normal','fontsize',15)
ylabel('\sigma(t)','fontsize',15)
xlabel('Time (sec)','fontsize',15)

%state convergence

xp1=x(:,1:5);
plot(t,x)
title('State Convergence','fontweight','normal','fontsize',15)
ylabel('States','fontsize',15)
xlabel('Time (sec)','fontsize',15)
```

A.4 Plot generation for LQR controller

```
xp1=x(:,1);
xp2=x(:,2);
xp3=x(:,3);
xp4=x(:,4);
xp5=x(:,5);

figure(1)
plot(t,xp1,'red')
hline = refline(0,0.);
     set(hline,'color','black');
     set(hline,'LineStyle','- -');
title('Position of state X','fontweight','normal','fontsize',15)
ylabel('State x','fontsize',15)
xlabel('Time (sec)','fontsize',15)
saveas(figure(1),'1.bmp');
hold on;
```

```
figure(2)
plot(t,xp2,'red')
hline = refline(0,0.);
     set(hline,'color','black');
     set(hline,'LineStyle','- -');

title('Velocity of state X','fontweight','normal','fontsize',15)
ylabel('Velocity of State x','fontsize',15)
xlabel('Time (sec)','fontsize',15)
saveas(figure(2),'2.bmp');
hold on;


figure(3)
plot(t,xp3,'red')
hline = refline(0,0.);
     set(hline,'color','black');
     set(hline,'LineStyle','- -');
title('Anglular Position of
theta','fontweight','normal','fontsize',15)
ylabel('Angular Position of theta','fontsize',15)
xlabel('Time (sec)','fontsize',15)
saveas(figure(3),'3.bmp');
hold on;


figure(4)
plot(t,xp4,'red')
hline = refline(0,0.);
     set(hline,'color','black');
     set(hline,'LineStyle','- -');
title('Anglular velocity of
theta','fontweight','normal','fontsize',15)
ylabel('Angular Velocity of theta','fontsize',15)
xlabel('Time (sec)','fontsize',15)
saveas(figure(4),'4.bmp');
hold on;


figure(5)
plot(t,xp5,'red')
hline = refline(0,0.);
     set(hline,'color','black');
     set(hline,'LineStyle','- -');
title('Actuator Dynamics','fontweight','normal','fontsize',15)
ylabel('Actuator Dynamics','fontsize',15)
xlabel('Time (sec)','fontsize',15)
saveas(figure(5),'5.bmp');
hold on;
```